REVIEW ARTICLE

Properties of the multiorbital Hubbard models for the iron-based superconductors

Elbio Dagotto[1,2,†], **Adriana Moreo**[1,2], **Andrew Nicholson**[1,2], **Qinglong Luo**[1,2], **Shuhua Liang**[1,2], **Xiaotian Zhang**[1,2]

[1] *Department of Physics and Astronomy, The University of Tennessee, Knoxville, TN 37996, USA*

[2] *Materials Science and Technology Division, Oak Ridge National Laboratory, Oak Ridge, TN 37831, USA*

E-mail: [†] *edagotto@utk.edu*

Received September 30, 2011; accepted November 6, 2011

A brief review of the main properties of multiorbital Hubbard models for the Fe-based superconductors is presented. The emphasis is on the results obtained by our group at the University of Tennessee and Oak Ridge National Laboratory, Tennessee, USA, but results by several other groups are also discussed. The models studied here have two, three, and five orbitals, and they are analyzed using a variety of computational and mean-field approximations. A "physical region" where the properties of the models are in qualitative agreement with neutron scattering, photoemission, and transport results is revealed. A variety of interesting open questions are briefly discussed such as: what are the dominant pairing tendencies in Hubbard models? Can pairing occur in an interorbital channel? Are nesting effects of fundamental relevance in the pnictides or approaches based on local moments are more important? What kind of magnetic states are found in the presence of iron vacancies? Can charge stripes exist in iron-based superconductors? Why is transport in the pnictides anisotropic? The discussion of results includes the description of these and other open problems in this fascinating area of research.

Keywords superconductivity

PACS numbers 74.20.Rp, 71.10.Fd, 74.70.Xa, 75.10.Lp

Contents

1 Introduction

1.1 Goals of this review

The discovery of a new family of high temperature superconductors based on Fe [1–8] has created considerable excitement in the condensed matter community. These new materials are intrinsically important because they appear to provide another example of non-BCS superconductors. In addition, it is expected that new clues towards solving the puzzle of the Cu-oxide high critical

temperature superconductivity will be achieved if a deep understanding of the Fe-based counterparts is reached. The present special volume contains a variety of important contributions to this topic covering several areas, and for this reason our contribution will focus specifically on the research carried out by the group of Profs. Moreo and Dagotto at the University of Tennessee and Oak Ridge National Laboratory, as of November 2011. Besides the authors of the present review, several other close collaborators provided many fundamental contributions to this effort, and all of them are properly cited here. In view of this focus on results by our present group and current and former collaborators, the Introduction will contain only a brief generic summary of the status of the Fe-based superconductors investigations, while the bulk of the publication will focus on our results using multiorbital Hubbard models to study theoretically the physics of these exciting compounds. It is important to remark that this manuscript is *not* intended as a full review of the theoretical studies of pnictides and chalcogenides. For this reason, the number of references is limited and, as already expressed, the results discussed are basically those of our group. However, the readers can easily reach most of the relevant publications on the subjects that are addressed here by simply consulting the cited literature, and the references therein. Another important warning for the readers is that the tone of this manuscript will be "informal" avoiding technicalities and focusing on the intuitive aspects of the results. However, once again, sufficient references are provided to help the readers to follow the technical aspects if they wish to penetrate deeper into the details of how the results were obtained.

1.2 Brief introduction to Fe-based phenomenology

A typical example of the Fe-based superconducting family of compounds is provided by $LaO_{1-x}F_x$ Fe As, one of the most studied pnictides in this area of research. The record superconducting critical temperature of ~ 55 K [7] has been achieved in a related compound SmO_{1-x}-F_xFeAs. These values for the critical temperatures are second only to those observed in the Cu-oxide family of high critical temperature superconductors. Indeed several aspects of the physics of the new Fe-based superconductors echoes the properties of the cuprates: (i) The cuprates are based on two dimensional planes containing a square lattice of Cu ions connected by O ions at the links [9]. Similarly, in the Fe-based superconductors the fundamental components in their structures are also layers defined by a square array of Fe atoms, but with atoms of other elements such as As, P, or Se, at the center of each Fe plaquette, alternating above or below the Fe layer. (ii) In both the cuprates and pnictides the parent compound of the material presents magnetic

order, although with different wavevectors (see below). (iii) Evidence of an exotic pairing mechanism (meaning non phononic) has been observed in the cuprates and also in the pnictides and chalcogenides [10–12]. (iv) The importance of Coulombic correlations between the electrons is crucial for the cuprates, opening for instance a Mott gap in the parent compound, and it has been considered also of considerable relevance for the pnictides in several investigations [13–23]. (v) The pairing state is, in both cases, a spin singlet [24–26]. (vi) In addition, similarly as in the cuprates, a pseudogap was detected in the pnictides [27–30].

On the other hand, both families of materials also differ in several aspects: (i) The parent compound is a Mott insulator in the cuprates, but it is a (bad) metal in the case of the pnictides (note that considerable excitement has been generated quite recently by the discovery of chalcogenide superconductors that appear to have insulators as parent compounds, as will be discussed elsewhere in this manuscript). (ii) In the magnetic ordered state of the cuprates, the Cu spins form an antiferromagnetic checkerboard arrangement while in the pnictides the spin of the Fe atoms are ordered antiferromagnetically in one Fe–Fe direction but ferromagnetically in the other. (iii) The Cu $3d_{x^2-y^2}$ is the orbital that mostly contributes to the Fermi surface (FS) of the cuprates, while both the Fe $3d_{xz}$ and $3d_{yz}$ form most of the FS surface of the pnictides and, moreover, several researchers argue that the contribution of the three remaining Fe 3d orbitals cannot be neglected. (iv) The cuprates have a single FS while the pnictides exhibit multiple FS's, which may include hole and electron-like pocket features. Note also that the cuprates show Fermi "arcs" (or Fermi "pockets") particularly in the underdoped regime, and thus far these exotic features have not been found in the pnictides. (v) There is clear experimental evidence showing that the pairing operator in the cuprates has d-wave symmetry and exhibits nodes at the FS. However, the symmetry of the pairing operator in the pnictides is controversial. On the experimental side, the results regarding the properties of the pairing operator seem to depend both on the material studied and on the experimental technique used. For example, several experimental investigations suggest the presence of nodes in the superconducting gap [24, 25, 31–39]. This is reminiscent of the nodes that appear in the d-wave superconducting state of the high-T_c cuprates. However, many other investigations indicate nodeless superconductivity [40–44]. On the theory front, several proposals for the dominant pairing tendencies, including s and d states, have been made [45–55].

To address the physics of these compounds theoretically *ab-initio* calculations based on the standard LDA approximation have been carried out, but this type of approach has limitations particularly if electronic corre-

lation effects are of some relevance. Moreover, certainly LDA cannot address the study of the superconducting tendencies and pairing channels since they are beyond the scope of those *ab-initio* methods. For this reason, at present considerable interest is focusing more and more into model Hamiltonians investigations. This brings an important new challenge with respect to previous studies for the cuprates: for the pnictides and chalcogenides a *multiorbital* approach is needed, considerably increasing the effort of computational studies. In fact, the analysis of "multiorbital Hubbard models" in general defines a new "grand challenge" for theoretical and computational many-body studies.

There are indications that the five 3d orbitals of the Fe should be included in a realistic model, but the practical need for unbiased tools, such as numerical calculations, must also be considered. For this reason, in this review several models for the pnictides, ranging from the simplest that includes only two orbitals, to a more elaborate one with three, and to the most sophisticated five-orbital cases will be presented. The rationale of the approach discussed here can be summarized as follows: (i) Perform a Lanczos study of the two-orbital model in a small cluster studying exactly the properties of the ground state. (ii) Use the results obtained numerically in the previous step to guide the use of mean-field approximations. (iii) Compare the mean-field results with the numerical results for the two-orbital model and tune parameters and details. (iv) Apply similar mean-field approximations to models with three, four, and five orbitals, that cannot be studied with Lanczos methods, and understand how the different properties depend on the number of orbitals. Of course, at every step a comparison with available experimental literature provides additional crucial information on the validity of the approach.

The organization of this brief review is simple. The two-orbital Hubbard model is reviewed first, followed by the three-orbital model, and in each case many results are discussed. Then, a variety of other interesting results are presented including charge stripe tendencies, relevance of nesting effects, magnetic order in the presence of Fe vacancies, anisotropies observed in the optical conductivity, and several others. Emphasis is on open problems and also plans for future calculations are discussed.

2 Two-orbital model

This "mini-review" of the research of our group will start with the case of the two-orbital Hubbard model. Other groups originally also presented such simple models, which are based on the Fe d_{xz} and d_{yz} orbitals [56]. And also several other groups have addressed the physics of this model for the new superconductors, using a vari-

ety of many-body approximations [57–67]. Detailed classifications of the possible superconducting order parameters for the two-orbital model have also been presented [68, 69]. However, as explained in the Introduction, the focus here will be the results presented by our group in this context.

2.1 Hopping terms

Based on a detailed analysis of the many possible "hopping" channels for electrons when only the two orbitals d_{xz} and d_{yz} are involved in the process, investigations based on the Slater–Koster approximation led to the construction of a tight-binding model Hamiltonian for this case [70]. The As atoms are merely considered as bridges between the Fe atoms. Thus, for the two-dimensional square lattice of irons, this "kinetic energy" portion of the Hamiltonian is given by

$$
\begin{aligned}
H_{\mathrm{TB}} = &-t_1 \sum_{\boldsymbol{i},\sigma}(d_{\boldsymbol{i},x,\sigma}^\dagger d_{\boldsymbol{i}+\hat{y},x,\sigma} + d_{\boldsymbol{i},y,\sigma}^\dagger d_{\boldsymbol{i}+\hat{x},y,\sigma} + h.c.) \\
&-t_2 \sum_{\boldsymbol{i},\sigma}(d_{\boldsymbol{i},x,\sigma}^\dagger d_{\boldsymbol{i}+\hat{x},x,\sigma} + d_{\boldsymbol{i},y,\sigma}^\dagger d_{\boldsymbol{i}+\hat{y},y,\sigma} + h.c.) \\
&-t_3 \sum_{\boldsymbol{i},\hat{\mu},\hat{\nu},\sigma}(d_{\boldsymbol{i},x,\sigma}^\dagger d_{\boldsymbol{i}+\hat{\mu}+\hat{\nu},x,\sigma} + d_{\boldsymbol{i},y,\sigma}^\dagger d_{\boldsymbol{i}+\hat{\mu}+\hat{\nu},y,\sigma} + h.c.) \\
&+t_4 \sum_{\boldsymbol{i},\sigma}(d_{\boldsymbol{i},x,\sigma}^\dagger d_{\boldsymbol{i}+\hat{x}+\hat{y},y,\sigma} + d_{\boldsymbol{i},y,\sigma}^\dagger d_{\boldsymbol{i}+\hat{x}+\hat{y},x,\sigma} + h.c.) \\
&-t_4 \sum_{\boldsymbol{i},\sigma}(d_{\boldsymbol{i},x,\sigma}^\dagger d_{\boldsymbol{i}+\hat{x}-\hat{y},y,\sigma} + d_{\boldsymbol{i},y,\sigma}^\dagger d_{\boldsymbol{i}+\hat{x}-\hat{y},x,\sigma} + h.c.) \\
&-\mu \sum_{\boldsymbol{i}}(n_{\boldsymbol{i}}^x + n_{\boldsymbol{i}}^y) \quad\quad\quad (1)
\end{aligned}
$$

where the operator $d_{\boldsymbol{i},\alpha,\sigma}^\dagger$ creates an electron at site $\boldsymbol{i}$ of the square lattice, at the orbital α, and with spin projection σ. The notation x and y is used for the two orbitals, instead of d_{xz} and d_{yz}. Some details are important to remark. For instance, note that the hopping is not only between nearest-neighbor (NN) atoms, but also along the plaquette diagonals, namely to next-NN (NNN) Here note that the notation in Eq. (1) is such that, for example, $\hat{x}$ denotes a unit vector along the x direction linking one site with its nearest neighbor, and a similar notation for the other direction. The reader should consult the original Ref. [70] to better comprehend the quite complex hopping structure of the model that involves not only NN and NNN terms but in addition hoppings that link both the same as well as different orbitals.

The presence of NN and NNN terms is easy to understand based on the fact that As, P, or Se, are located in the middle of the plaquettes (actually slightly above or below the Fe plane, alternatively), contrary to the oxygens in cuprates that are in the middle of the Cu-Cu link. This simple geometrical factor related with the

crystal structure immediately brings the issue of "spin frustration" into the table. For instance, in the strong coupling limit of large Hubbard U (with the explicit form of this interaction to be defined below in the three-orbital model section), NN hoppings would generate only NN spin Heisenberg terms, but the NNN contributions will generate frustrating NNN spin interactions. This is important, since it is for this basic reason, namely the comparable importance of the NN and NNN hopping terms, that the wavevector of relevance in the magnetic state of the pnictides is $(\pi, 0)$ instead of (π, π) as in the cuprates. It is well known that a Heisenberg interaction with NN and NNN terms displays a ground state with wavevector $(\pi, 0)$ (degenerate with $(0, \pi)$) when the NNN coupling is comparable or larger than the NN coupling [71]. Note that this rationale is based on a spin model that can be defined in the strong U coupling limit, while in weak coupling the notion of "nesting" (to be addressed briefly later) provides an alternative simple explanation.

With regards to the specific values of the hopping amplitudes, in our early efforts they were derived from the Slater–Koster formalism that establishes a relation between the hoppings and some particular overlaps of atomic wave functions [70]. But another simpler approach, widely used, is to simply fit the values of the many hopping amplitudes by means of a comparison with angle-resolved photoemission experiments or band structure calculations.

For the case of the Slater–Koster approach, and using generic values for the wave function overlaps and some energy gaps that appear in the SK formalism, the band structure and Fermi surface of the model are shown in Fig. 1. Considering how crude this approach is, the fact that the final result contains hole pockets at the Γ point and electron pockets at the X and Y points, as the pnictides do, is remarkable. Again, it is the geometry of the problem, i.e., of the crystal structure, that rapidly locates us into a multi Fermi surface "environment" for
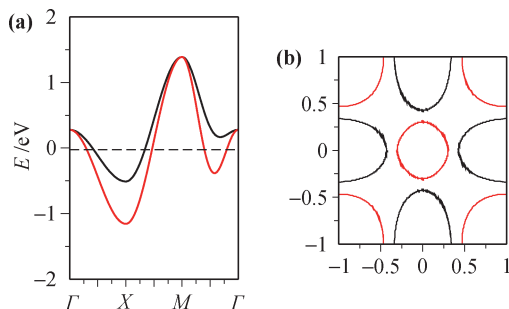
the pnictides, without the need of carrying out LDA calculations. However, note that the FS of this model in the SK approximation is only qualitatively correct, since the size of the pockets is too large when compared with other more numerically realistic (and complicated) approaches.

Other authors have used the philosophy of simply fitting hopping amplitudes against band structure or photoemission results, as already explained. Results from Ref. [56] are in Fig. 2. In this case note that the Fermi surface is qualitatively similar to that of Fig. 1 but the size of the pockets are smaller. Also note that the overall bandwidths are quite different between the two sets of hoppings, but since most of the physics arises from states near the Fermi level, at least at weak and intermediate couplings, this discrepancy is not important. Also note that at energies of more than 1 eV corrections from other Fe orbitals and other atoms are of much relevance, thus comparing actual bandwidths is not crucial.
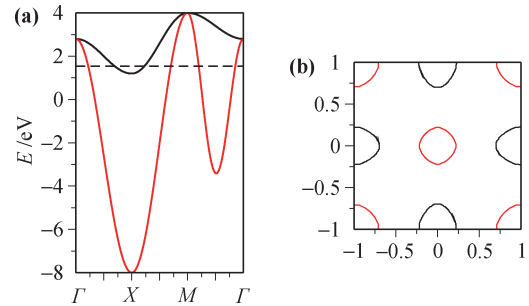

Fig. 2 **(a)** Energy vs. momentum for the non-interacting two-orbital tight-binding Hamiltonian described in this section using the hopping amplitudes obtained from fits of band-structure calculations [56]. The actual hoppings are $t_1 = -1.0$, $t_2 = 1.3$, and $t_3 = t_4 = -0.85$ (all in eV units). Results are plotted along the path $(0, 0) - (\pi, 0) - (\pi, \pi) - (0, 0)$. **(b)** Fermi surface for the half-filled system. Reproduced from Ref. [70], Copyright © 2009 American Physical Society.

2.2 Results for the two-orbital model

As discussed before, the importance of the NNN hoppings in the tight-binding portion of the Hamiltonian is a clear indicator that the magnetic state of the undoped limit (which for two orbitals means two electrons per Fe) may have magnetic tendencies that are not like those of Cu oxides. In fact, after adding the Hubbard interactions (that will be provided explicitly below for the case of three orbitals) calculations using the Lanczos method (shown in Fig. 3) clearly indicate that the spin structure factor presents a peak at wavevectors $(\pi, 0)$ and $(0, \pi)$, as opposed to (π, π). Notice that the wavevectors that are dominant in the two orbital model are those of relevance in the case of the real pnictide compounds, according to neutron scattering results [72]. It is interesting that even the simplest of the multiorbital models for the pnictides, namely using just two orbitals as opposed to five, already provides the correct wavevector for the magnetic order.

Fig. 1 **(a)** Energy vs. momentum for the non-interacting tight-binding two-orbital Hamiltonian in Eq. (1) using $t_1 = 0.058$ eV, $t_2 = 0.22$ eV, $t_3 = -0.21$ eV, and $t_4 = -0.08$ eV. These hopping amplitudes are obtained from the Slater–Koster formulas as described in Ref. [70]. Results are plotted along the path $(0, 0) - (\pi, 0) - (\pi, \pi) - (0, 0)$. **(b)** Fermi surface for the half-filled system. Reproduced from Ref. [70], Copyright © 2009 American Physical Society.
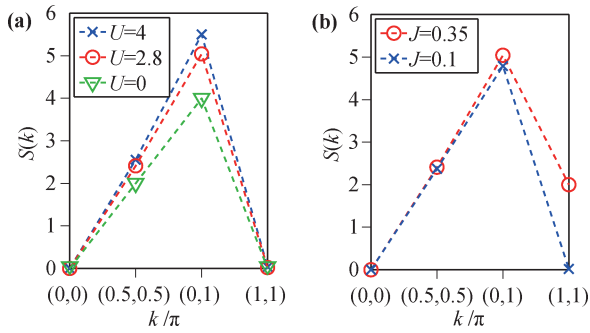
Fig. 3 Spin structure factor $S(k)$ obtained for the case of hopping parameters $t_1 = -1.0$, $t_2 = 1.3$, $t_3 = t_4 = -0.85$ (in eV units) [56], using the two-orbital Hubbard model. **(a)** are results for several values of the Hubbard on-site repulsion U and the Hund coupling (in units of eV) $J/U = 1/8$; **(b)** results for two values of J, with $U = 2.8$ eV fixed. (a) and (b) were obtained at half filling using the Lanczos method (i.e., these are exact results) on $\sqrt{8} \times \sqrt{8}$ clusters. Reproduced from Ref. [70], Copyright © 2009 American Physical Society.

The analysis of the two-orbital Hubbard model also included the calculation of the one-particle spectral function [73], which is shown in Fig. 4. The technique used to carry out this calculation is the Hartree mean-field approximation. The results suggest that there are two critical values of the Hubbard U coupling where qualitative changes occur. At large U, panel (c), it is clear

that there is a large gap, indicating an insulating state. This is reasonable in the large U limit. At small U, panel (a), the Fermi surface is the same as at $U = 0$ since the mean-field order parameter is found to be zero in a finite range of small U. The most interesting result is shown in the intermediate panel (b), which corresponds to intermediate U. In this case, some of the bands that crossed the Fermi level in the non interacting limit now develop a gap, while others not. So this corresponds to a partial gap opening of the Fermi surface. Since, as will be shown explicitly for more orbitals, in this regime the magnetic order parameter is nonzero, then this intermediate range of U contains a state that is simultaneously *magnetic* and *metallic*, as in pnictide experiments [70, 73].

Associated with the results described before for the one-particle spectral function are the momentum-integrated density of states (DOS), shown in Fig. 5. The actual calculation of these DOS's was carried out using the VCA technique (Variational Cluster Approx.). For details the reader should consult Ref. [73] and references therein. The important point is that the DOS shows the presence of three regimes: no gap at $U = 0$, "pseudo-gap" at intermediate U, and a large full gap at large U, in agreement with the one-particle spectral function of the previous figure.

Fig. 5 VCA calculated density-of-states for different values of U in the metallic regime (with both good metal and pseudogap behaviors, for the nonmagnetic and magnetic cases, respectively) and insulating regimes of the two-orbital Hubbard model, using the SK hopping parameters and $J = U/4$. Reproduced from Ref. [73], Copyright © 2009 American Physical Society.
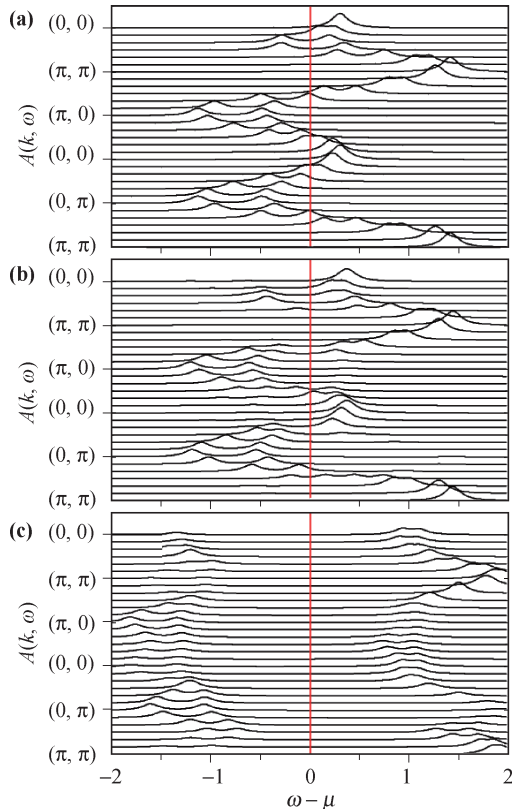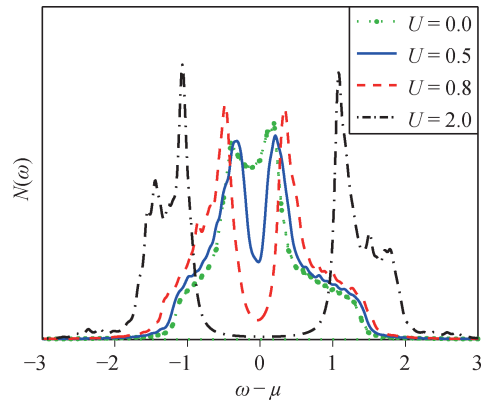

Fig. 4 Two-orbital model mean-field spectral function along high symmetry directions in the extended First Brillouin Zone, using the model with SK hoppings [67]. The different panels correspond to different values of U: **(a)** $U = 0.5$, **(b)** $U = 0.8$, **(c)** $U = 2.0$ (all in eV units). The Hund coupling is fixed to $J = U/4$ and the magnetic order wavevector is $(\pi, 0)$. Reproduced from Ref. [73], Copyright © 2009 American Physical Society.

Overall, the study of the two-orbital Hubbard model using a combination of Lanczos and mean-field techniques provided results that were in surprising qualitative agreement with experiments for pnictides: the correct experimental Fermi surface at high temperature can be obtained by tuning the hopping amplitudes, the correct wavevector for magnetic order spontaneously appears in the Lanczos method, and the presence of a "bad metal" at intermediate couplings is suggested by the pseudogap nature of the DOS at those couplings.

Before turning to the three-orbital model, note that it is difficult to carry out calculations at finite temperature

with the mean-field approximation, particularly in the regime near the critical temperature for antiferromagnetism. Moreover, *above* the critical temperature in this formalism there are no remnants of any form of magnetism, not even local moments. However, as will be discussed in the section related with "nesting", recent experiments strongly suggest the presence of local moments above the ordering temperature, showing that the pnictides are likely in an intermediate coupling regime where weak coupling procedures are qualitative at best.

3 Three-orbital model

While the two-orbital model described before has several properties that are in good agreement with experiments, it is known that the Fermi surface of the pnictides has a d_{xy} component at the electron pockets. For this reason it is important to propose a tight-binding model with three orbitals (xz, yz, and xy), and with a Fermi surface that is in agreement with photoemission and band calculations, not only with regards to its shape but also its orbital composition.

3.1 Real space

A three-orbital Hubbard model for the pnictides has been proposed in Ref. [74]. Following the Slater–Koster procedure described in Ref. [70], the mathematical form of this tight-binding model can be established, and then the hopping amplitudes are obtained by fitting results for the Fermi surface against photoemission experiments. The explicit form for this model is given below. NN and diagonal NNN hoppings were considered for all the orbitals. It is clear that the hopping terms for the xz and yz orbitals are the same as in the previously discussed two-orbital model and they are here repeated for completeness:

$$H^{xz,yz} = -t_1 \sum_{\boldsymbol{i},\sigma}(d^\dagger_{\boldsymbol{i},xz,\sigma}d_{\boldsymbol{i}+\hat{y},xz,\sigma}+d^\dagger_{\boldsymbol{i},yz,\sigma}d_{\boldsymbol{i}+\hat{x},yz,\sigma}+h.c.)$$

$$-t_2 \sum_{\boldsymbol{i},\sigma}(d^\dagger_{\boldsymbol{i},xz,\sigma}d_{\boldsymbol{i}+\hat{x},xz,\sigma} + d^\dagger_{\boldsymbol{i},yz,\sigma}d_{\boldsymbol{i}+\hat{y},yz,\sigma} + h.c.)$$

$$-t_3 \sum_{\boldsymbol{i},\hat{\mu},\hat{\nu},\sigma}(d^\dagger_{\boldsymbol{i},xz,\sigma}d_{\boldsymbol{i}+\hat{\mu}+\hat{\nu},xz,\sigma}+d^\dagger_{\boldsymbol{i},yz,\sigma}d_{\boldsymbol{i}+\hat{\mu}+\hat{\nu},yz,\sigma}+h.c.)$$

$$+t_4 \sum_{\boldsymbol{i},\sigma}(d^\dagger_{\boldsymbol{i},xz,\sigma}d_{\boldsymbol{i}+\hat{x}+\hat{y},yz,\sigma} + d^\dagger_{\boldsymbol{i},yz,\sigma}d_{\boldsymbol{i}+\hat{x}+\hat{y},xz,\sigma} + h.c.)$$

$$-t_4 \sum_{\boldsymbol{i},\sigma}(d^\dagger_{\boldsymbol{i},xz,\sigma}d_{\boldsymbol{i}+\hat{x}-\hat{y},yz,\sigma} + d^\dagger_{\boldsymbol{i},yz,\sigma}d_{\boldsymbol{i}+\hat{x}-\hat{y},xz,\sigma} + h.c.)$$

$$-\mu \sum_{\boldsymbol{i}}(n_{\boldsymbol{i},xz} + n_{\boldsymbol{i},yz}) \tag{2}$$

With regards to the new intra-orbital hoppings for the xy orbital, these hopping terms are given by

$$H^{xy} = t_5 \sum_{\boldsymbol{i},\hat{\mu},\sigma}(d^\dagger_{\mathbf{i},xy,\sigma}d_{\boldsymbol{i}+\hat{\mu},xy,\sigma} + h.c.)$$

$$-t_6 \sum_{\boldsymbol{i},\hat{\mu},\hat{\nu},\sigma}(d^\dagger_{\boldsymbol{i},xy,\sigma}d_{\boldsymbol{i}+\hat{\mu}+\hat{\nu},xy,\sigma} + h.c.)$$

$$+\Delta_{xy} \sum_{\boldsymbol{i}} n_{\boldsymbol{i},xy} - \mu \sum_{\boldsymbol{i}} n_{\mathbf{i},xy} \tag{3}$$

where Δ_{xy} is the energy difference between the xy and the degenerate xz/yz orbitals. Finally, the hybridization terms between the xz/yz and the xy orbitals are the following:

$$H^{xz,yz;xy} = -t_7 \sum_{\boldsymbol{i},\sigma}[(-1)^{|\mathrm{i}|}d^\dagger_{\boldsymbol{i},xz,\sigma}d_{\boldsymbol{i}+\hat{x},xy,\sigma} + h.c.]$$

$$-t_7 \sum_{\boldsymbol{i},\sigma}[(-1)^{|\mathrm{i}|}d^\dagger_{\boldsymbol{i},xy,\sigma}d_{\boldsymbol{i}+\hat{x},xz,\sigma} + h.c.]$$

$$-t_7 \sum_{\boldsymbol{i},\sigma}[(-1)^{|\mathrm{i}|}d^\dagger_{\boldsymbol{i},yz,\sigma}d_{\boldsymbol{i}+\hat{y},xy,\sigma} + h.c.]$$

$$-t_7 \sum_{\boldsymbol{i},\sigma}[(-1)^{|\mathrm{i}|}d^\dagger_{\boldsymbol{i},xy,\sigma}d_{\boldsymbol{i}+\hat{y},yz,\sigma} + h.c.]$$

$$-t_8 \sum_{\boldsymbol{i},\sigma}[(-1)^{|\mathrm{i}|}d^\dagger_{\boldsymbol{i},xz,\sigma}d_{\boldsymbol{i}+\hat{x}+\hat{y},xy,\sigma} + h.c.]$$

$$+t_8 \sum_{\boldsymbol{i},\sigma}[(-1)^{|\mathrm{i}|}d^\dagger_{\boldsymbol{i},xy,\sigma}d_{\boldsymbol{i}+\hat{x}+\hat{y},xz,\sigma} + h.c.]$$

$$-t_8 \sum_{\boldsymbol{i},\sigma}[(-1)^{|\mathrm{i}|}d^\dagger_{\boldsymbol{i},xz,\sigma}d_{\boldsymbol{i}+\hat{x}-\hat{y},xy,\sigma} + h.c.]$$

$$+t_8 \sum_{\boldsymbol{i},\sigma}[(-1)^{|\mathrm{i}|}d^\dagger_{\boldsymbol{i},xy,\sigma}d_{\boldsymbol{i}+\hat{x}-\hat{y},xz,y\sigma} + h.c.]$$

$$-t_8 \sum_{\boldsymbol{i},\sigma}[(-1)^{|\mathrm{i}|}d^\dagger_{\boldsymbol{i},yz,\sigma}d_{\boldsymbol{i}+\hat{x}+\hat{y},xy,\sigma} + h.c.]$$

$$+t_8 \sum_{\boldsymbol{i},\sigma}[(-1)^{|\mathrm{i}|}d^\dagger_{\boldsymbol{i},xy,\sigma}d_{\boldsymbol{i}+\hat{x}+\hat{y},yz,\sigma} + h.c.]$$

$$+t_8 \sum_{\boldsymbol{i},\sigma}[(-1)^{|\mathrm{i}|}d^\dagger_{\boldsymbol{i},yz,\sigma}d_{\boldsymbol{i}+\hat{x}-\hat{y},xy,\sigma} + h.c.]$$

$$-t_8 \sum_{\boldsymbol{i},\sigma}[(-1)^{|\mathrm{i}|}d^\dagger_{\boldsymbol{i},xy,\sigma}d_{\boldsymbol{i}+\hat{x}-\hat{y},yz,\sigma} + h.c.]$$

$$\tag{4}$$

The operator $d^\dagger_{\boldsymbol{i},\alpha,\sigma}$ ($d_{\boldsymbol{i},\alpha,\sigma}$) creates (annihilates) an electron at site $\boldsymbol{i}$, orbital $\alpha = xz, yz, xy$, and with spin projection σ. $n_{\boldsymbol{i},\alpha} = n_{\boldsymbol{i},\alpha,\uparrow} + n_{\boldsymbol{i},\alpha,\downarrow}$ are the corresponding density operators. As discussed before, the entire set of hopping parameters t_i in Eqs. (2)–(4) will be determined by fitting the band dispersion of the model to band structure calculation or photoemission results. The chemical potential μ is set to a two-thirds filling, which corresponds to four electrons per Fe site. At this electronic density, the Fermi surface is in agreement with experiments. Previously proposed three-orbital models [50, 75] only contained the NN hybridization t_7, but since NNN terms are included for the intra-orbital component, as

well as for the hybridization between xz and yz, they should also be included in the hybridization with xy. It can be shown that these NNN terms with hopping t_8 turn out to be very important to provide the proper orbital character for the electron pockets when compared with LDA results. Finally note that the hybridization Eq. (4) contains factors $(-1)^{|\mathbf{i}|}$ that arise from the two-iron unit cell of the original FeAs planes. The explicit values for the hoppings are provided in Table 1, reproduced from [74].

Table 1 Parameters for the tight-binding portion of the three-orbital model. The overall energy unit is electron volts. For more details see Ref. [74], where additional information for a better visualization of the hoppings is provided.

t_1	t_2	t_3	t_4	t_5	t_6	t_7	t_8	Δ_{xy}
0.02	0.06	0.03	−0.01	0.2	0.3	−0.2	$-t_7/2$	0.4

The hopping term in the Hamiltonian can be transformed to momentum space and diagonalized. Explicit expressions can be found in Ref. [74]. The results for the band structure (see Fig. 6) show that the hopping amplitudes mentioned above provide a Fermi surface in qualitative agreement with experiments. Moreover, the orbital composition is also in agreement with band structure calculations, that includes the dominance of the xy component in small portions of the electron-pocket Fermi surfaces.
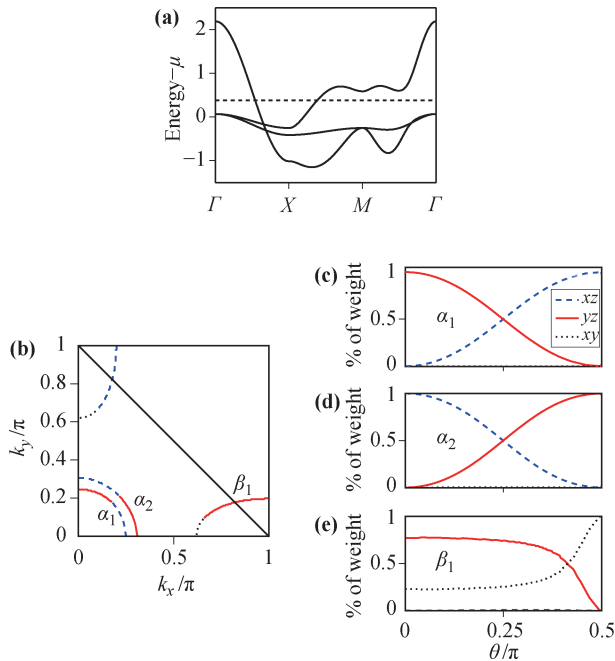

Fig. 6 **(a)** Band structure and Fermi surface of the tight-binding (i.e., non-interacting) three-orbital model, with parameters from Table 1 and in the unfolded BZ. The diagonal thin solid line in **(b)** indicates the boundary of the folded BZ. In panels **(c)**–**(e)**, the orbital compositions of the two hole and one of the electron pockets are given. The winding angle θ is measured with respect to the k_y-axis. The second electron pocket is analogous to the one shown simply replacing xz by yz. In all panels, the dashed lines refer to the xz orbital, the solid to yz, and the dotted to xy. Reproduced from Ref. [74], Copyright © 2010 American Physical Society.

3.2 Coulombic interactions

The Coulombic interacting portion of the three-orbital Hamiltonian is given by

$$
\begin{aligned}
H_{\text{int}} = &\ U \sum_{\mathbf{i},\alpha} n_{\mathbf{i},\alpha,\uparrow} n_{\mathbf{i},\alpha,\downarrow} + (U' - J/2) \sum_{\mathbf{i},\alpha<\beta} n_{\mathbf{i},\alpha} n_{\mathbf{i},\beta} \\
&- 2J \sum_{\mathbf{i},\alpha<\beta} \mathbf{S}_{\mathbf{i},\alpha} \cdot \mathbf{S}_{\mathbf{i},\beta} \\
&+ J \sum_{\mathbf{i},\alpha<\beta} (d^\dagger_{\mathbf{i},\alpha,\uparrow} d^\dagger_{\mathbf{i},\alpha,\downarrow} d_{\mathbf{i},\beta,\downarrow} d_{\mathbf{i},\beta,\uparrow} + h.c.)
\end{aligned}
\tag{5}
$$

where $\alpha, \beta = 1, 2, 3$ denote the orbitals, $\mathbf{S}_{\mathbf{i},\alpha}$ ($n_{\mathbf{i},\alpha}$) is the spin (electronic density) of orbital α at site $\mathbf{i}$ (this index labels sites of the square lattice defined by the irons), and the relation $U' = U - 2J$ between the Kanamori parameters has been used (for a discussion in the context of manganites see Ref. [76]). The first two terms give the energy cost of having two electrons located in the same orbital or in different orbitals, both at the same site, respectively. The second line contains the Hund's rule coupling that favors the ferromagnetic (FM) alignment of the spins in different orbitals at the same lattice site (note that the Hund coupling will be denoted by J or by J_{H} in this review, because both notations are often used). The "pair-hopping" term is in the third line and its coupling is equal to J by symmetry. Although it was not provided explicitly, the Hubbard interaction for the case of other number of orbitals (such as two, discussed before) is the immediate generalization of the case of three orbitals shown here.

Note that the values used for U and J can be substantially smaller than the atomic ones, because the interactions may be screened by bands not included in the Hamiltonian. This comment is also valid for the values of physical relevance when models with different number of orbitals are considered. The Coulomb interaction terms introduced above have been used and discussed in several previous publications [67, 70, 73, 74, 77] where more details can be found by the readers. All energies are provided here in electron volts, unless otherwise stated. As already expressed, and as shown in Ref. [74], the electronic density of relevance for the three-orbital Hubbard model is $n = 4$ per site (i.e., 4 electrons spread into the 3 orbitals of each site) to reproduce the expected Fermi surface in the paramagnetic regime.

3.3 Mean-field approximation

To study the ground state properties of the models introduced before, a mean-field approximation can be applied. This approximation was discussed in publications for two orbitals [73, 77] that the reader can consult for more details. The simple standard assumption of considering only the mean-field values for the diagonal opera-

tors follows [78]:

$$\langle d^{\dagger}_{\boldsymbol{i},\mu,\sigma} d_{\boldsymbol{j},\nu,\sigma'}\rangle = \left[n_{\mu} + \frac{\sigma}{2}\cos(\boldsymbol{q}\cdot\boldsymbol{r_i})m_{\mu}\right]\delta_{\boldsymbol{ij}}\delta_{\mu\nu}\delta_{\sigma\sigma'} \quad (6)$$

where $\boldsymbol{q}$ is the ordering wavevector of the magnetic order. n_{μ} and m_{μ} are mean-field parameters (to be determined self-consistently) describing the charge density and magnetization of the orbital μ, respectively. The rest of the notation is standard. Applying Eq. (6) to the Hubbard portion of the Hamiltonian, the full mean-field Hamiltonian in momentum space can be written as

$$H_{\mathrm{MF}} = H_{\mathrm{TB}} + C + \sum_{\boldsymbol{k},\mu,\sigma} \epsilon_{\mu} d^{\dagger}_{\boldsymbol{k},\mu,\sigma} d_{\boldsymbol{k},\mu,\sigma}$$
$$+ \sum_{\boldsymbol{k},\mu,\sigma} \eta_{\mu,\sigma}(d^{\dagger}_{\boldsymbol{k},\mu,\sigma} d_{\boldsymbol{k+q},\mu,\sigma} + d^{\dagger}_{\boldsymbol{k+q},\mu,\sigma} d_{\boldsymbol{k},\mu,\sigma})$$
$$(7)$$

where $\boldsymbol{k}$ runs over the extended first BZ, H_{TB} is the hopping term in momentum space, the constant C is

$$C = -NU\sum_{\mu}\left(n_{\mu}^2 - \frac{1}{4}m_{\mu}^2\right) - N(2U'-J)\sum_{\mu\neq\nu}n_{\mu}n_{\nu}$$
$$+ \frac{NJ}{2}\sum_{\mu\neq\nu}m_{\mu}m_{\nu}$$

N is the number of sites, and the following definitions were introduced

$$\epsilon_{\mu} = Un_{\mu} + (2U'-J)\sum_{\nu\neq\mu}n_{\nu} \quad (8)$$

$$\eta_{\mu,\sigma} = -\frac{\sigma}{2}\left(Um_{\mu} + J\sum_{\nu\neq\mu}m_{\nu}\right) \quad (9)$$

The mean-field Hamiltonian can be numerically solved for a fixed set of mean-field parameters using standard library subroutines to diagonalize the fermionic sector. n_{μ} and m_{μ} are obtained self-consistently by minimizing the energy via an iterative process. During the iterations $\sum_{\mu}n_{\mu} = n$ was enforced at each step, such that the total charge density per site is a constant (4 for the three-orbital model, 6 for the five-orbital model, and 2 for the two-orbital model). Note also that the numerical solution of the mean-field Hamiltonian immediately allows for the calculation of the band structure, density of states (DOS), and magnetization ($m = \sum_{\mu}m_{\mu}$) at the ordering wavevector $\boldsymbol{q}$, and many other quantities.

3.4 Results for the three-orbital model

The complete three-orbital model (hopping and Coulombic terms) cannot be studied in the same eight-sites cluster where the two-orbital model was exactly solved using the Lanczos method. Thus, mean-field approximations must be used from the start to obtain some information about this model. Some results are shown in Fig. 7, working at electronic density of four electrons per Fe

site, and varying the couplings U and J/U. From this figure, it is clear that there are many competing states. At small U, there is no magnetic order and the state is paramagnetic. With increasing U, a variety of magnetic orders develop including a region dominated by a "realistic" region with $(\pi,0)$ wavevector, that happened to be orbitally disordered. With further increasing U, a variety of insulating states are observed with different wavevectors for magnetism and with different arrangements for orbital order. Overall, qualitative features of the two-orbital model survive in the sense of having basically three regimes of small, intermediate, and large U couplings (with transport characteristics being metal, poor metal, and insulator, respectively). However, the presence of a third orbital induces a richer variety of combinations for the spin and orbital degrees of freedom.
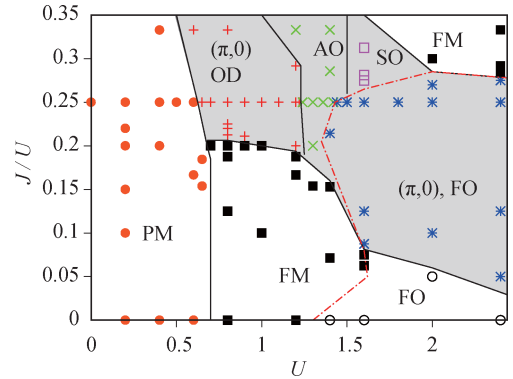

Fig. 7 Qualitative phase diagram of the three-orbital Hubbard model in the mean-field approximation, varying the J/U and U couplings. The shaded area denotes the stability region of the realistic $(\pi,0)$ magnetic ordering. The lines are guides to the eye, the dot-dashed line approximately indicates the metal-insulator transition. The data points were obtained by comparing the energies of the various phases within the mean-field approximation. The meaning of the symbols is the following: +: $(\pi,0)$-AF state without pronounced orbital order (orbital disorder, OD); ×: $(\pi,0)$-AF state with (π,π) alternating orbital (AO) order with $\phi = 0$; empty squares: $(\pi,0)$-AF state with $(0,\pi)$ orbital stripes (SO) ($\phi = 0$); ∗: $(\pi,0)$-AF state with ferro-orbital (FO) order ($\phi = 0$); filled squares: FM with FO ordering tendencies, $\phi = \pi/4$. This FO order is weaker for small U and larger $J \approx 0.2$. The filled circles denote parameters that do not support magnetically ordered states. For small J, some FO order with $\phi = \pi/4$ is found, similar to the FM phase. The empty circles at large U and small J denote similar states without magnetic ordering, but with extreme orbital order, where the xy orbital is (almost) empty, while xz and yz are (almost) filled. Reproduced from Ref. [74], Copyright © 2010 American Physical Society.

Another interesting issue in the context of multiorbital models is the possibility of orbital order. The phase diagram of the three-orbital model shows that indeed orbital order can happen, although that usually occurs at large U where the system is an insulator. But what is the situation at intermediate couplings in the realistic region for pnictides that is simultaneously magnetic and metallic? Figure 8(a) shows the contribution of each orbital to the magnetization of the $(\pi,0)$ state. At large U it is clearly different for the three orbitals, indicating orbital

order. However, at intermediate U there are still some small differences between xz and yz. The same with regards to the orbital occupation in panel (b), although with an even smaller difference between xz and yz at intermediate couplings. For more details see Ref. [74].
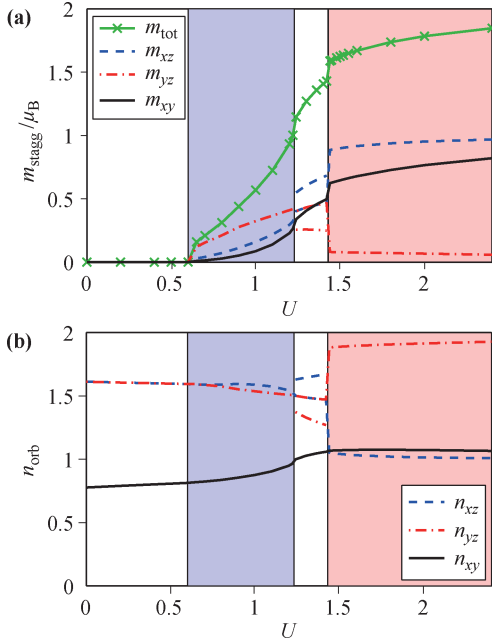

Fig. 8 **(a)** Orbital magnetization and **(b)** orbital occupation number as a function of the on-site Hubbard repulsion strength U, obtained with a mean-field approximation applied to the three-orbital Hubbard model. The colors indicate the different phases that with increasing U are: uncorrelated metal, itinerant $(\pi, 0)$ antiferromagnet without orbital order, itinerant $(\pi, 0)$ antiferromagnet with alternating orbital order, and a ferro-orbitally-ordered $(\pi, 0)$ antiferromagnetic insulator. Hopping parameters are from Table 1, and $J = U/4$. Reproduced from Ref. [74], Copyright © 2010 American Physical Society.

Why is that at intermediate couplings there are visible differences between the contributions to the magnetization of the xz and yz orbitals even if the state is not orbitally ordered? The reason is that at low temperatures the magnetic state $(\pi, 0)$ breaks rotational invariance, thus breaking explicitly the symmetry between the two orbitals. But once a full integration over energy is carried out to produce the total occupation of each orbital, the differences seen at the Fermi surface become much smaller [79]. This can be visualized in Fig. 9 where the DOS is shown for the xz and yz orbitals. Clearly the DOS of the yz orbital presents a drastic reduction (pseudogap) at the Fermi level due to the opening of gaps at the original Fermi surface, mainly due to nesting effects. Thus, at intermediate couplings there is a weaker form of orbital order that occurs at the Fermi surface, but that is not true orbital order in the long-range sense. This important conceptual topic is of relevance in the interpretation of experiments that only focus on Fermi surface physics.

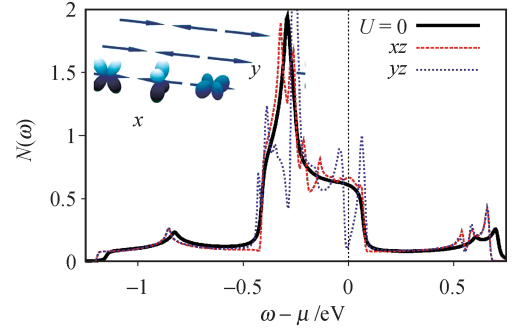Figure 10 contains information about the magnetic

Fig. 9 Density of states of the xz and yz orbitals in the $(\pi, 0)$-AF phase of the three-orbital model at $U = 0.7$ and $J = U/4$, studied with the mean-field approximation. For these values of U and J, the orbital densities are $n_{xz} = n_{xz,\uparrow} + n_{xz,\downarrow} = 1.590 \approx n_{yz} = 1.586$, and the magnetizations $m_{xz} = n_{xz,\uparrow} - n_{xz,\downarrow} = 0.04 \ll m_{yz} = 0.15$. For $U = 0$, the DOS $N(\omega)$ is identical for both orbitals (solid line). A Gaussian broadening with $\sigma = 0.005$ was used. The inset illustrates the $(\pi, 0)$-AF order considered here and the xz, yz, and xy orbitals (left to right). Reproduced from Ref. [79], Copyright © 2010 American Physical Society.

order for wavevector $(\pi, 0)$ vs. U, parametric with J/U. At small J/U, including zero, there is a discontinuity at a value of U different from that where the magnetization develops. Thus, as expected from the one-particle spectral-function analysis of the two-orbital model, there is an intermediate coupling regime, between two critical values of U, where the dominant state is simultaneously magnetic and metallic (the latter property arising from the DOS).
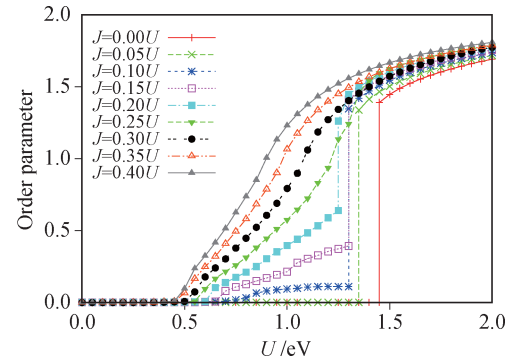

Fig. 10 Mean-field order parameter at wavevector $(\pi, 0)$ vs. U (in eV units) for the three-orbital Hubbard model, and parametric with the values of J/U indicated. Reproduced from Ref. [80], Copyright © 2010 American Physical Society.

For the case of the three-orbital Hubbard model the band structure and Fermi surface has been calculated within the mean-field approximation and the results are reproduced in Figs. 11 and 12. As U grows, it is clear that "satellite" structures develop at the Fermi surface, in agreement with angle-resolved photoemission experiments (for a detailed list of references see Ref. [80]) in the low-temperature magnetic state. More detail about the satellite peaks, and their hole vs. electron character, can be seen in Fig. 12.

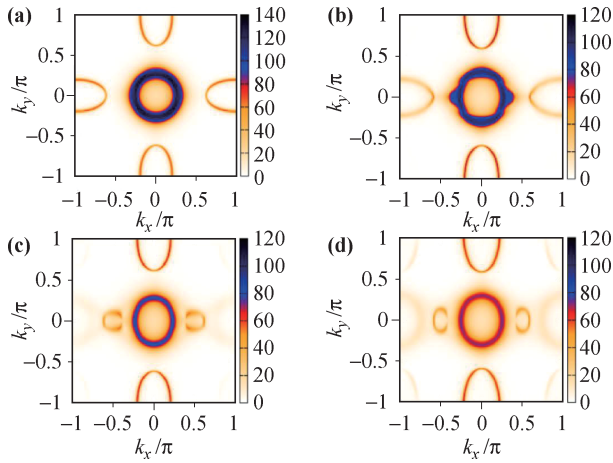The comparison between mean-field approximation results and neutron scattering and photoemission

Fig. 11　Unfolded mean-field Fermi surfaces for the three-orbital model corresponding to (m = order parameter) **(a)** $U = 0$, as reference (there are two hole pockets at Γ but they appear merged due to the broadening used for plotting); **(b)** $J/U = 0.33$, $U = 0.6$, $m = 0.2$; **(c)** $J/U = 0.20$, $U = 1.0$, $m = 0.4$; and **(d)** $J/U = 0.25$, $U = 1.05$, $m = 0.6$. Reproduced from Ref. [80], Copyright © 2010 American Physical Society.
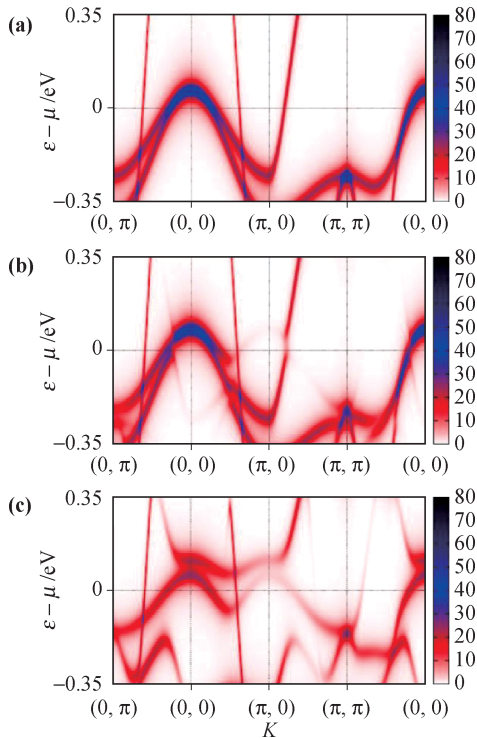

Fig. 12　Unfolded band structure mean-field results for the three-orbital Hubbard model and cases **(a)** $U = 0$, as reference; **(b)** $J/U = 0.33$, $U = 0.6$, $m = 0.2$; and **(c)** $J/U = 0.25$, $U = 1.05$, $m = 0.6$. Panels (b) and (c) show a V-shaped pocket in between the $(0,0)$ and $(\pi,0)$ points. The scale used (arbitrary units) is on the right of the panels. Reproduced from Ref. [80], Copyright © 2010 American Physical Society.

experiments, supplemented by the constraint that the parent compounds of pnictides are metallic, imposes severe constraints on the values of coupling constants of relevance for the pnictides. The results are in Fig. 13. The range of J/U is centered at $1/4$ and the value of U is centered at 1 eV for the three-orbital model.
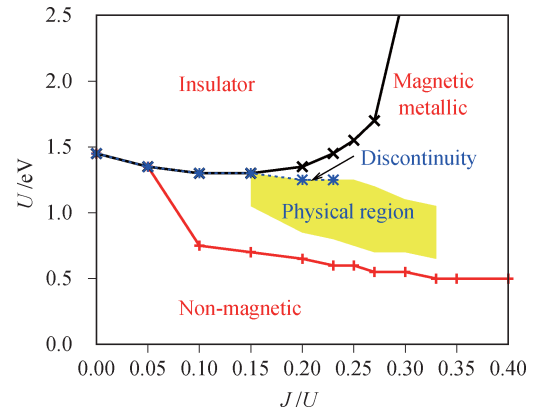

Fig. 13　Phase diagram for the three-orbital Hubbard model obtained with the mean-field approximation. The "physical region" shown in yellow is the regime of couplings found to be compatible with neutron and photoemission experiments. The "non-magnetic" region corresponds to a regime where the state has a zero order parameter. In the "insulator" region, there is no Fermi surface and the state is insulating. The "discontinuity" label corresponds to the discontinuous jump in the order parameter shown in Fig. 10. The entire "magnetic metallic" regime could in principle have been compatible with experiments, but only in the yellow highlighted region is that m is sufficiently small-intermediate in value to match neutrons and the Fermi surface has satellite pockets near the Γ-point hole pockets to match photoemission results. Reproduced from Ref. [80], Copyright © 2010 American Physical Society.

Summarizing both the results of this Section and the previous one, we can see clearly that the two- and three-orbital Hubbard models provide a reasonable starting point to the physics of the pnictides, since a range of couplings can be found that matches several experimental results for these materials. The rest of this manuscript will now be devoted to a variety of topics that are conceptually interesting and where several open issues remain to be answered.

4　Are there charge stripes in models for pnictides?

In the area of the high critical temperature superconductors based on Cu, there is an active subfield of research that relies on the possible existence of charge stripes, which is a charge inhomogeneous state reached by hole doping the insulator parent compound. These stripes are basically made of parallel lines of holes, aligned either in one direction or another of the Cu-oxide layers, with the undoped antiferromagnetic state in between [81]. Can a similar phenomenon occur in pnictides? At first sight this seems unlikely because one of the main reasons for the stripes in cuprates is the robust antiferromagnetic order in the undoped limit: when charge is added (holes) to this background, each individual hole distorts the magnetic state in its vicinity and to reduce this "damage" the holes must be arranged together. Coulomb repulsion prevents a large cluster of holes, thus the optimal situation is the charge stripes. But the pnictides are located at intermediate Hubbard U couplings, so the situation

in that context is less clear.

Early calculations in cuprates that predicted the existence of stripes relied on mean-field approximations (Hartree–Fock) [82–85]. Thus, it is natural to apply exactly the same technique but now to the two-orbital Hubbard model. Moreover, there are some experimental indications of nematic behavior in pnictides [86, 87], thus the search for possible reasons for these anisotropies are important. The calculation for stripes in pnictides was carried out by members of our group and the results were reported in Ref. [88], and some results are reproduced in this section. In Fig. 14, results using the Hartree–Fock approximation in real space, namely allowing each of the expectation values in the HF Hamiltonian to vary independently from site to site, are shown. These results are reached via an iterative process starting typically with random numbers for the many expectation values to prevent biasing the results toward a particular solution.

Figure 14 shows the presence of charge stripe states in the two-orbital Hubbard model for pnictides, when the system is doped with extra electrons. Note the clear presence of two lines of charge where the extra electrons accumulate. Note also in the other panel that the spin order is such that the spin stripes, as opposed to the charge stripes, are oriented along the other direction. Moreover, at the location of the charge stripes interesting domain walls are formed. For more details see Ref. [88].
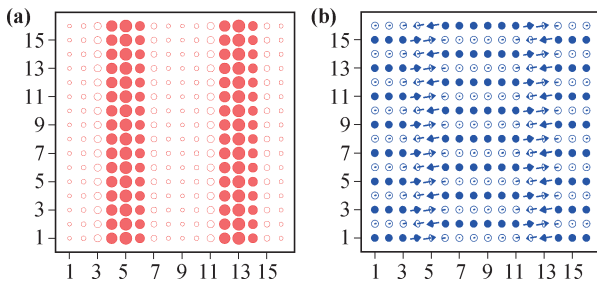

Fig. 14 **(a)** Example of charge-striped state found in the HF approximation to the two-orbital model, using the hoppings of Refs. [67, 70], overall electronic density $\langle n \rangle = 2.33$, $U = 0.8$, $J_H/U = 0.25$, and a 16×16 cluster. The size of the circles is linearly related to the charge, with the largest circles denoting $n_{max} = 2.42$ and the smallest $n_{min} = 2.27$. Full (open) circles are used when the local density is larger (smaller) than the average. **(b)** Mean value of the spin in the state shown in (a). Note the presence of domain walls at the location of the charge stripes, inserted in a mainly $(0, \pi)$ background. For more details the readers should consult Ref. [88] from where this figure is reproduced.

Figure 15(a) provides another example of the charge stripes found in HF investigations for the two-orbital Hubbard model. Panel (b) shows that the effect occurs for hole doping, similarly as in the previously shown results for electron doping. Panel (d) illustrates the density vs. chemical potential curves and the associated size effects which in this case appear to be small. Panel (c) is perhaps the most important since among many quantities it contains the "Δn" which is the difference between the charge value inside and outside the stripes. The fact

that this number is different from zero even in a region where the gap is zero in the undoped limit suggests that stripes may even exist when the extra carriers are added to the intermediate coupling metallic–magnetic state believed to be of relevance for pnictides. This is a conceptually novel state not described before in the cuprates since in that context it was the Mott insulator that was being doped.
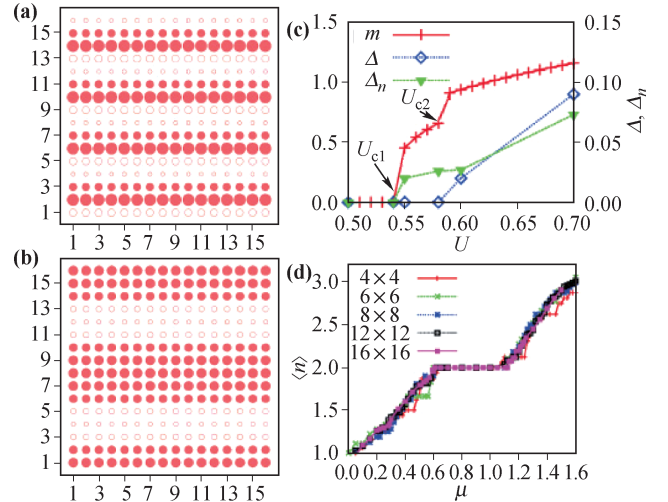

Fig. 15 **(a)** HF charge-striped state using the hopping amplitudes of Refs. [67, 70], at $\langle n \rangle = 2.45$, $U = 0.8$, and $J_H/U = 0.25$. The size of the circles is proportional to the charge, with $n_{max} = 2.48$ and $n_{min} = 2.41$. **(b)** Same as (a) but for $\langle n \rangle = 1.83$, $U = 1.0$, with $n_{max} = 1.84$ and $n_{min} = 1.81$. **(c)** $(\pi, 0)$ antiferromagnetic order parameter m, charge gap Δ (from $\langle n \rangle$ vs. μ), and $\Delta n = n_{max} - n_{min}$ at $\langle n \rangle \sim 2.3$, as a function of U. U_{c1} is the critical U where magnetism starts while U_{c2} is the critical U where a gap develops in the density of states. **(d)** $\langle n \rangle$ vs. μ at $U = 1.0$, $J_H/U = 0.25$, and various lattice sizes, suggesting that size effects are small in this quantity. Results at others U's appear equally well converged. Reproduced from Ref. [88], Copyright © 2011 American Physical Society.

In spite of the potential important relevance of these results, it is fair to remark that still much more work is needed to confirm the existence of charge stripe states in Hubbard models for pnictides. Among several potentially important improvements, HF calculations with additional orbitals should be carried out to confirm the presence of these stripes beyond the two-orbital model. The reader is encouraged to consult the original reference [88] for more details and also for citations about experimental work that reported spin incommensurate order in real pnictides: this type of spin order is very natural in charge stripe states and it may provide an evidence for stripe formation (but Fermi surface effects can also lead to spin incommensurate order without charge stripes). As explained before, also there have been reports of nematic order in pnictides (see Refs. [86, 87]) that are compatible with charge stripes. However, it is still too early to claim that indeed charge stripes do exist in doped pnictides. Also it is too early to address even more subtle issues such as whether these charge stripes compete with superconductivity or instead they facili-

tate the stabilization of such a state. Clearly, much more work is needed to fully understand these difficult issues.

5   Competition of pairing tendencies in the two-orbital Hubbard model

The issue of the existence of pairing tendencies in Hubbard models has been controversial since the early days of research in cuprates, over 20 years ago [9]. While there are solid arguments that suggest pairing in purely electronic Hubbard models, the evidence of this pairing is not conclusive in square lattices, although it is convincing in two-leg ladder systems [89]. Different is the situation if variations of the Hubbard model are used such as the famous t–J model [9]. In this case the Heisenberg coupling J is considered a free parameter, as opposed to being $J = 4t^2/U$ as in the strong coupling limit of the Hubbard model (t is the hopping of the one-band Hubbard model), and, thus, the tendencies towards a robust magnetic order can be enhanced by increasing J. In the t–J model several calculations have shown that pairing in the famous d-wave channel of cuprates is indeed present in the model, both in two-leg ladders and in square lattices [9, 89].

What is the situation in the area of the Fe-based superconductors? Here the problem is "worse" since the multiorbital nature of the problem makes the calculations much more difficult. To make progress in this area recently a Lanczos calculation was setup, namely an exact solution of the Hubbard model for two orbitals was found, for a small cluster of just eight sites [90]. This tiny system still has millions of states in the Hilbert space, thus justifying the severe size limitation in the calculation. How can pairing be studied in this small cluster? As discussed above, a trick to increase the pairing tendencies is to use a t–J model but such a model is not known yet in the area of pnictides (our group and collaborators did calculate the analytic form of this model but it is very cumbersome and such model has not been fully analyzed yet). Thus, a simpler route is to merely add a Heisenberg interaction term to the Hubbard model, still allowing for doubly occupied orbitals to appear in the Hilbert space but with a J coupling (actually in practice both NN and NNN couplings, denoted by J_{NN} and J_{NNN}, respectively) that can be increased to make the magnetic tendencies more robust (note also that the notation "J" is used for the Hund coupling of the multiorbital Hubbard model as well, so the reader should be cautious in deducing from the context if "J" denotes a Heisenberg NN coupling or an on-site Hund coupling). By this procedure, namely increasing J_{NN} and J_{NNN}, the binding of two extra electrons added to the "undoped" parent compound limit can be studied [90]. Of main interest in this calculation is what is the pairing channel (i.e., s, d, p) of relevance in

these systems. While plenty of calculations in pnictides have been already carried out analyzing the properties of isolated pairing channels, only unbiased calculations such as the one sketched here, limited as it is, can truly address their competition. For the case of cuprates a similar small cluster calculation gave clear evidence that d-wave was the only channel of relevance in cuprates [9]. What is the situation for pnictides? After all, there are many conflicting reports of nodal vs. nodeless superconductivity in these compounds.

Some of the results of this difficult calculation, that involved the diagonalization of the eight-site cluster thousands of times [90], are reproduced in Fig. 16. The left panel illustrates tendencies when in the absence of the extra Heisenberg couplings. The most important results are in the right panel, where the different tendencies for pairing are shown varying the Hubbard and Hund couplings. The three colors denote three different channels. At large Hund coupling there are tendencies toward a spin triplet state, but experimentally this is unlikely. Thus, the most interesting results are those in blue and red. They show two competing tendencies: s wave vs. d wave. Actually the two irreducible representations of the D_{4h} point group involved in the process are A_{1g} and B_{2g}, respectively. A special case of the former is the $s^{\pm}$ state that has been much discussed in pnictides, although in most of the blue region the superconducting gap has some wavevector dependent structure, namely it is more generic than the plain $s^{\pm}$. With regards to B_{2g}, this seems to be a competing channel that was observed already in some of our previous publications with regards
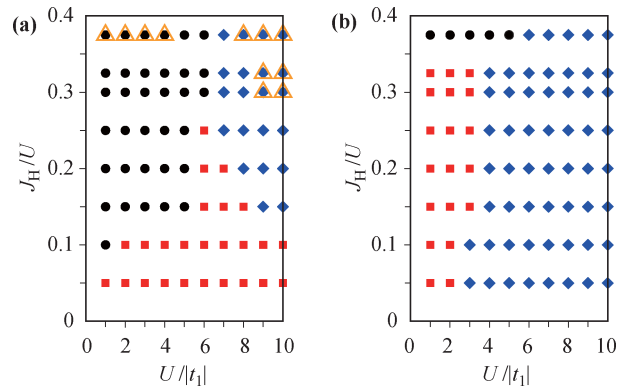

Fig. 16 Study of the pairing tendencies of the two-orbital Hubbard model on small clusters (eight sites) studied exactly via the Lanczos algorithm. Shown is the relative symmetry between the $N = 16$ (undoped) and $N = 18$ ground states, varying U and J_H/U (with N the number of electrons). Circles denote triplet states, squares B_{2g}-symmetric singlets, and diamonds A_{1g}-symmetric singlets. **(a)** Results for the special case where the extra couplings that render the system a "t–U–J" model, with stronger magnetic tendencies, vanish i.e., $J_{NN} = J_{NNN} = 0$ for comparison. Open triangles indicate binding but this occurs only in small regions of parameter space. **(b)** Results now with nonzero J_{NN} and J_{NNN}. Shown are the different pairing channels, each for the lowest value of (J_{NN}, J_{NNN}) where binding appears. Results reproduced from Ref. [90] where more details about the notation and calculations can be found.

to the actual quantum numbers of the state of two extra electrons for the two-orbital Hubbard model [67]. However, only in the calculation shown in Fig. 16(b) is that a true bound state is observed. The overall qualitative conclusion of this effort is that contrary to the cuprates, there seems to be more than one pairing tendency in the two-orbital model for pnictides, and depending on the actual couplings different specific members of the pnictide family could be located in one case or the other.

However, note that much more work is needed to confirm these results. In particular, it is at present not clear to what extent the presence of the d-wave competing state is also a property of more realistic three- or five-orbital models. This issue will be very difficult to clarify in the future since the size of the Hilbert spaces are too large to repeat the same calculation for the case of three or more orbitals. Thus, for the time being it is imperative that the possibility of pairing channels other than s-wave be further considered in experimental studies of pnictides. The reader interested in these topics should consult Ref. [90] for more details and references about this fascinating subject.

6 Are interorbital pairing tendencies possible in two-band models?

As remarked in the investigations described in the previous section, there are competing tendencies for pairing, at least within the two-orbital model. Within the spin singlet sector, the competition between d and s arises from the existence of the orbital degrees of freedom. For the case of d-wave (B_{2g}) the operator that creates the pair is interorbital, i.e., the two electrons of the Cooper pair do not belong to the same orbital, but to different ones. To address qualitatively the issue of interband pairing in the pnictides, and to move beyond the traditional Hubbard model into more phenomenological models, in recent investigations the following two-bands simplified model with interband pairing was considered [91]:

$$H_{\bm{k}} = \sum_{\alpha,\sigma} \epsilon_\alpha(\bm{k}) c^\dagger_{\bm{k},\alpha,\sigma} c_{\bm{k},\alpha,\sigma} + V \sum_{\alpha\neq\beta} (c^\dagger_{\bm{k},\alpha,\uparrow} c^\dagger_{-\bm{k},\beta,\downarrow} + h.c.)$$

(10)

where $\alpha, \beta, = 1, 2$ label two bands that are not hybridized, σ is the spin projection, and for simplicity

$$\epsilon_\alpha(\bm{k}) = \frac{-\bm{k}^2}{2m_\alpha} + C$$

(11)

which gives parabolic bands that are degenerate at $\bm{k} = 0$ with energy C, and with a chemical potential $\mu = 0$. This can be considered as a crude representation of the two hole-pocket bands around the Γ point in the pnictides, but more importantly this model defines a simple toy model where the effects of interband pairing can be stud-

ied. In general, the parameter $V = V_0\Delta$ in the second term, where pairing is favored by hand, can be considered as the product of an attractive potential V_0 between electrons in the two different bands and a mean-field parameter Δ determined by minimizing the total energy.

In order to study at what values of the coupling the interband pair is formed, let us assume that the, more fundamental, interaction term responsible for the interband attraction is given by

$$H_{\mathrm{attr}} = \frac{1}{N} \sum_{\bm{k},\bm{k}'}, \alpha V_{\bm{k},\bm{k}'} c^\dagger_{\bm{k},\alpha,\uparrow} c^\dagger_{-\bm{k},-\alpha,\downarrow} c_{-\bm{k}',-\alpha,\downarrow} c_{\bm{k}',\alpha,\uparrow}$$

(12)

where $V_{\bm{k},\bm{k}'} = -V_0$ and N is the number of sites. Performing the standard mean-field approximation: $b_{\bm{k}'} = \langle c_{-\bm{k}',-\alpha,\downarrow} c_{\bm{k}',\alpha,\uparrow}\rangle$ and $b^\dagger_{\bm{k}} = \langle c^\dagger_{\bm{k},\alpha,\uparrow} c^\dagger_{-\bm{k},-\alpha,\downarrow}\rangle$ and making the substitution $c^\dagger_{\bm{k},\alpha,\uparrow} c^\dagger_{-\bm{k},-\alpha,\downarrow} = b^\dagger_{\bm{k}} + (c^\dagger_{\bm{k},\alpha,\uparrow} c^\dagger_{-\bm{k},-\alpha,\downarrow} - b^\dagger_{\bm{k}})$ (and an analogous substitution for the product of annihilation operators), the mean-field results were obtained. Defining $\Delta = \frac{1}{N}\sum_{\bm{k}} b_{\bm{k}} = \frac{1}{N}\sum_{\bm{k}} b^\dagger_{\bm{k}}$ the following mean-field Hamiltonian was reached:

$$H_{\mathrm{MF}} = \sum_{\alpha,\sigma} \epsilon_\alpha(\bm{k}) c^\dagger_{\bm{k},\alpha,\sigma} c_{\bm{k},\alpha,\sigma}$$
$$- V_0\Delta \sum_{\bm{k},\alpha\neq\beta} (c^\dagger_{\bm{k},\alpha,\uparrow} c^\dagger_{-\bm{k},\beta,\downarrow} + h.c.) + 2V_0\Delta^2 N$$

(13)

which is of the form shown before in Eq. (10). The minimization of the mean-field Hamiltonian shows that indeed superconductivity in the interband channel can be stabilized but with the only requirement that the pairing attraction cannot be simply infinitesimal, but a finite threshold must be crossed in order to reach the superconducting state (see Fig. 17). Thus, to the extent that the pairing in pnictides is sufficiently robust, then this phenomenological approach as well as the Lanczos calculations suggest that interband pairing (i.e., pairing
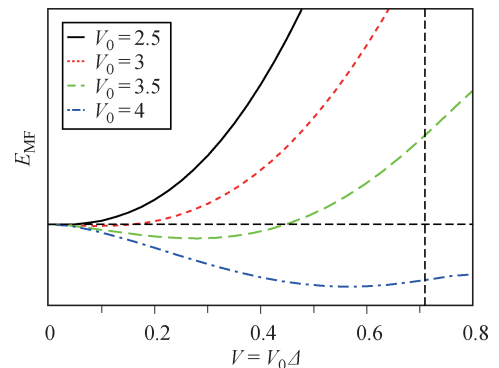

Fig. 17 Mean-field energy [expectation value of Eq. (13)] per site with interband pairing having strength $V_0/2$ vs. $V = V_0\Delta$, for different values of V_0. After a critical coupling of the pair attraction is reached, then superconductivity in the interband channel is stable. For more details and notation the reader should consult Ref. [91].

involving different orbitals) is actually possible in the Fe-based superconductors. For more details see Ref. [91].

7   Is nesting truly important?

In the early days of pnictides, it was widely assumed that nesting properties of the Fermi surface were important, first to develop the $(\pi, 0)$ magnetic order and then for the pairing tendencies. However, as investigations in this area of research progressed, this perception has lost some of its appeal. For instance, while 1111 materials with a small magnetic order parameter (according to neutron scattering results) could be located in the weak coupling regime, the 122 materials with a larger order parameter certainly need a larger U, although still in the intermediate U range of Hubbard couplings. The most recent developments (see next section) suggest the existence of parent compounds that are insulators, effectively increasing the values of U that appear to be of relevance in pnictides. In addition, recent experiments clearly show the existence of local moments above the ordering critical temperatures [92, 93]. This behavior is not expected in a weak-coupling approach where the moments are formed together with the development of long-range order. Then, to what extend nesting based scenarios are still relevant?

To qualitatively study nesting effects, in our recent publication [94] two models with virtually identical Fermi surfaces (with hole and electron pockets) were studied. The first model is actually the same two-orbital model for pnictides widely studied before and described already in this manuscript. For the purposes of the nesting investigation this is called the d-model. The other model was introduced in Ref. [94] and it is referred to as the s-model. It is formed by two non-hybridized bands or orbitals that happened to have the same FS as the d-model, but the composition of the hole pocket is 100% one band (or orbital) while the electron pocket is 100% the other.

The discussion in Ref. [94] is very detailed and readers are encouraged to consult this reference. Here, it will only be stated that both models eventually converge to similar magnetic states (for the parent compound) with the proper wavevector $(\pi, 0)$, as shown in Fig. 18. Thus, an important conclusion is that observing such a magnetic state experimentally is *not* sufficient to conclude that nesting ideas work since for the s-model the same state is reached for sufficiently large U. For the s-model there is an apparent nesting, but the wavevector $(\pi, 0)$ does not connect Fermi surface states with the same orbital composition, thus nesting effectively does not occur for this model. Knowing the actual orbital composition of the Fermi surface is crucial for any nesting-based argument.

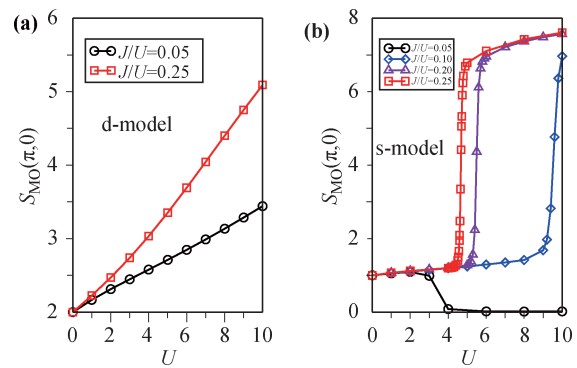In carrying out these calculations, it was observed that

Fig. 18 Orbital magnetic structure factor at wave vector $(\pi, 0)$ calculated numerically (Lanczos), reproduced from [94]. **(a)** Results for the two-orbital Hubbard model defined elsewhere in this manuscript that is here called d-model, as a function of the Coulomb repulsion U and for the values of J/U indicated. **(b)** Same as (a) but for the s-model defined in [94] (see also main text here). Both models eventually lead to the same magnetic order at large U with the proper wavevector for pnictides but the d-model develops this order rapidly in weak coupling due to nesting, while the s-model needs to reach a robust value of U to stabilize a qualitatively similar state.

the s-model developed a novel form of magnetism which is schematically shown in Fig. 19, in the same weak coupling regime where the d-model develops the nesting-based $(\pi, 0)$ state. This novel state presents order, but the net magnetic moment at each site cancels because the orientation of the spin at one orbital is the opposite as the spin in the other orbital. However, it is obvious to the eye that the states in Fig. 19 display an ordered state, namely the spins are developed and they are not randomly oriented. The reader should consult Ref. [94] for more details of this fascinating new state.
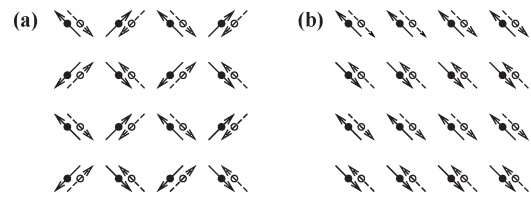

Fig. 19 Schematic representation of the real-space mean-field calculated ground states for the s-model when m_{12} is non-zero (see Ref. [94] for the notation): **(a)** Flux phase; **(b)** Magnetic stripe phase. The black and white dots represent the orbitals + and − at each site and the continuous and dashed arrows represent the MF value of the spin at each orbital. Reproduced from Ref. [94], Copyright © 2011 American Physical Society.

8   Fe-based superconductors with an insulator as parent compound?

One of the most interesting recent developments in Fe-based superconductors is the realization that some of the superconducting compounds have an insulator as a parent compound, as opposed to a bad metal. The chemical formula of a prominent representative of this tendency is $K_{0.8}Fe_{2-x}Se_2$. Whether the insulator observed in this context is a Mott or band insulator is too early to say.

Moreover, a variety of results suggest that there are vacancies in the FeSe planes, that for $x = 0.4$ form a regular $\sqrt{5} \times \sqrt{5}$ pattern. Neutron scattering results indicate that the 2×2 plaquettes that are defined by this Fe vacancy arrangement are ferromagnetically ordered and with a large magnetic moment, and with an antiferromagnetic effective coupling between them. The reader can consult Refs. [95–100], and references therein, for more details. Several theoretical results have been presented addressing this interesting state at $x = 0.4$. A partial list is [101–106]. In our effort in this area, to be described right below, a detailed comparison with the results of these previous theoretical papers can be found. Here, only the main results presented originally in Ref. [107] will be briefly reviewed.

Figure 20 displays the state found in the neutron scattering research for this compound that also appears prominently in our recent investigations using the Hartree–Fock approximation in real space [107]. The other two states are competitors that are very close in the phase diagram found in Ref. [107].
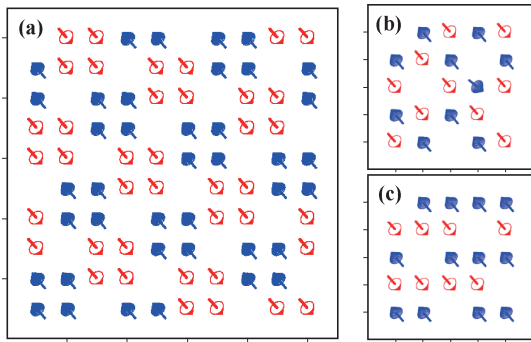

Fig. 20 **(a)** Sketch of the so-called "AF1" state found to be stable in a robust region of the $U - J/U$ phase diagram in our HF approximation to the five-orbital Hubbard model, in agreement with neutron diffraction [97]. **(b)** A competing state dubbed "AF4" (stable at smaller J/U's in the next figure). **(c)** The C competing state. For (b) and (c), a subset of the 10×10 cluster used is shown. More information can be found in the original reference [107].

Figure 21 is the phase diagram found in our investigations of the five-orbital Hubbard model [107]. The experimentally revealed state [97] dubbed "AF1" is prominent in a similar region of J/U that was previously referred to as the "physical region", namely where other previous efforts have shown that the results of the Hubbard model are also in agreement with neutron and photoemission efforts [80]. With regards to the actual values of U, as opposed to a ratio J/U, they are somewhat larger for the AF1 state than for the magnetic metallic state of the pnictides [80] (see previous sections in this same contribution for more details).

The effort reviewed here is just the beginning of a much more detailed investigation currently ongoing. Many questions arise, including the role of the vacancies in stabilizing the state found here, and to what extend
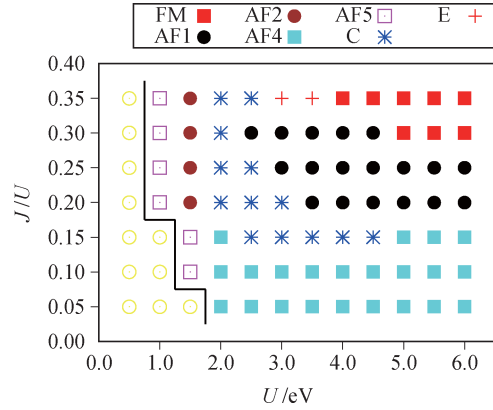

Fig. 21 Phase diagram of the five-orbital Hubbard model with $\sqrt{5} \times \sqrt{5}$ Fe vacancies studied via the real-space HF approximation to a 10×10 cluster, employing the procedure for convergence described in the original text [107]. With increasing U, clear tendencies toward magnetic states are developed. The realistic AF1 state found in neutron scattering experiments [97] appears here above $J/U = 0.15$ and for U larger than 2.5 eV. The notation for the most important states is explained in Fig. 20 and for the rest in Refs. [103, 104]. The region with low-intensity yellow circles at small U is non-magnetic. For more details the readers can consult the original reference [107].

this state should be labeled Mott or band insulator. Also, is this insulator truly the parent compound of the superconductors that are very close in the phase diagram? What are the optical and photoemission properties of this interesting state? Certainly our group will devote much more work to these topics in the near future.

9 Study of the anisotropy of pnictides via the optical conductivity

One of the most intriguing experimental results unveiled in the study of pnictides is the existence of an unexpected anisotropy in transport properties discovered in detwinned single crystals of doped and undoped AFe_2As_2, with A=Ba,Sr,Ca. The effect is the largest at low doping $x \sim 2\%$–4% in $Ba(Fe_{1-x}Co_x)_2As_2$ but it exists even in the undoped limit $x = 0$. Details of these experimental results can be found in Refs. [108–110]. Several theoretical publications have been devoted to this topic [111, 112]. Members of our group [113] have recently studied the optical conductivity of the three-orbital Hubbard model [74] using mean-field techniques, and indeed observed the presence of an anisotropy, mainly caused by the fact that near the Fermi surface there is an asymmetry in the population of the xz and yz orbitals induced by the magnetic order with wavevector $(\pi, 0)$ that already breaks rotational invariance [79]. The proposed explanation is more elaborated than this simple statement and the readers can find details and additional references in Ref. [113]. Here only a brief summary of the main results is provided.

Following well-known computational studies of $\sigma(\omega)$ in the context of the cuprates [9], the paramagnetic current operators in the two directions of a two-dimensional layer representing the Fe planes are defined as

$$\hat{j}_x = \sum_{\langle \boldsymbol{i},\boldsymbol{l}=\hat{\boldsymbol{x}},\hat{\boldsymbol{x}}+\hat{\boldsymbol{y}},\hat{\boldsymbol{x}}-\hat{\boldsymbol{y}}\rangle} \sum_{\alpha,\beta,\sigma} -\mathrm{i}t_{\boldsymbol{il}}^{\alpha\beta}(c_{\boldsymbol{i},\alpha,\sigma}^{\dagger} c_{\boldsymbol{i}+\boldsymbol{l},\beta,\sigma} - h.c.)$$

$$\hat{j}_y = \sum_{\langle \boldsymbol{i},\boldsymbol{l}=\hat{\boldsymbol{y}},\hat{\boldsymbol{x}}+\hat{\boldsymbol{y}},-\hat{\boldsymbol{x}}+\hat{\boldsymbol{y}}\rangle} \sum_{\alpha,\beta,\sigma} -\mathrm{i}t_{\boldsymbol{il}}^{\alpha\beta}(c_{\boldsymbol{i},\alpha,\sigma}^{\dagger} c_{\boldsymbol{i}+\boldsymbol{l},\beta,\sigma} - h.c.)$$

(14)

while the kinetic energy operators are

$$\hat{T}_x = \sum_{\langle \boldsymbol{i},\boldsymbol{l}=\hat{\boldsymbol{x}},\hat{\boldsymbol{x}}+\hat{\boldsymbol{y}},\hat{\boldsymbol{x}}-\hat{\boldsymbol{y}}\rangle} \sum_{\alpha,\beta,\sigma} t_{\boldsymbol{il}}^{\alpha\beta}(c_{\boldsymbol{i},\alpha,\sigma}^{\dagger} c_{\boldsymbol{i}+\boldsymbol{l},\beta,\sigma} + h.c.)$$

$$\hat{T}_y = \sum_{\langle \boldsymbol{i},\boldsymbol{l}=\hat{\boldsymbol{y}},\hat{\boldsymbol{x}}+\hat{\boldsymbol{y}},-\hat{\boldsymbol{x}}+\hat{\boldsymbol{y}}\rangle} \sum_{\alpha,\beta,\sigma} t_{\boldsymbol{il}}^{\alpha\beta}(c_{\boldsymbol{i},\alpha,\sigma}^{\dagger} c_{\boldsymbol{i}+\boldsymbol{l},\beta,\sigma} + h.c.)$$

(15)

using a standard notation. The total current, up to the first order term in the external field $\boldsymbol{A} = (A_x, A_y)$, can be written as $\hat{J}_x = (\hat{j}_x + \hat{T}_x A_x)/N$ and $\hat{J}_y = (\hat{j}_y + \hat{T}_y A_y)/N$. The real part of the optical conductivity in the x direction can be calculated following the steps detailed in Ref. [9]. From the well-known $\sigma(\omega)$ sum-rule, it can also be shown that the Drude weight in the x direction D_x is given by [9]

$$\frac{D_x}{2\pi} = \frac{\langle \phi_0 | -\hat{T}_x | \phi_0 \rangle}{2N} - \frac{1}{N}\sum_{n\neq 0} \frac{|\langle \phi_0 | \hat{j}_x | \phi_n \rangle|^2}{E_n - E_0}$$

(16)

where ϕ_0 is the many-body ground state, in this case the mean-field state with $(\pi, 0)$ magnetic order, and ϕ_n represents the many-body excited states, also produced in the mean-field calculation, with E_0 and E_n their corresponding energies. The optical conductivity and Drude weight in the y direction can be obtained and expressed similarly. N is the number of sites. In our calculation, the Dirac δ functions that appear in the expression for $\sigma(\omega)$ were regularized as a Lorentzian $\delta(\omega) \approx (1/\pi)\epsilon/(\omega^2 + \epsilon^2)$ with a small but finite broadening parameter ϵ.

The optical conductivity calculated in the mean-field approximation following the steps described above is shown in Fig. 22. It is clear that there is an anisotropy, namely the two directions are not equivalent. Actually, the direction that is ferromagnetic has a smaller zero-frequency weight than the antiferromagnetic direction, a result that may be found to be intuitively difficult to understand since studies in manganites often show that a ferromagnetic spin arrangement is better for transport. The reader should consult Ref. [113] for a discussion on why this intuition fails in the present case.

The Drude weights in the two directions are given in Fig. 23, and they explicitly show the anisotropy that appears qualitatively similar to that reported in experiments, in the range of couplings where the state is
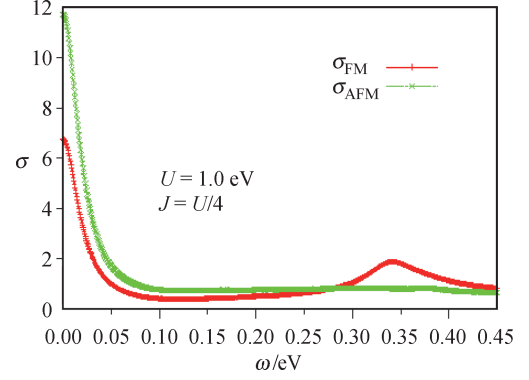

Fig. 22 The optical conductivity $\sigma(\omega)$ in the "physical region" [80] of the three-orbital model ($\epsilon = 0.02$). The unit of $\sigma(\omega)$ is $e^2/\hbar$. The couplings are $U = 1.0$ eV and $J = U/4$. The AFM direction (i.e., the x direction for magnetic wavevector $(\pi, 0)$) has a larger zero frequency conductivity than the FM direction, as found in experiments (cited in main text). The FM direction also has a peak at a finite frequency $\sim J$. Reproduced from Ref. [113], Copyright © 2011 American Physical Society.

simultaneously magnetic and metallic. Thus, the overall conclusion is that in the "physical region" of the three-orbital Hubbard model, the optical conductivity at low temperature is found to reproduce the experiments, adding to the good agreement found when results were compared against neutron scattering and angle-resolved photoemission techniques.
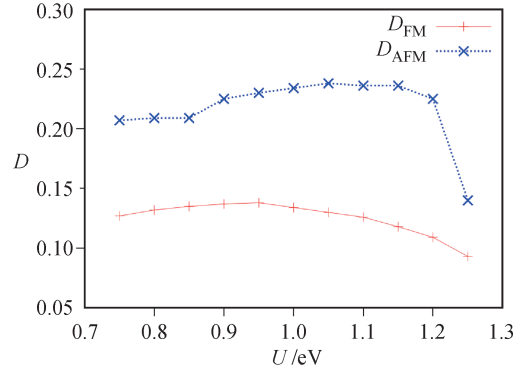

Fig. 23 Drude weight/π vs. U in the "physical region" [80] of the three-orbital model, at $J = U/4$. In this regime, the inequality $D_{\mathrm{AFM}} > D_{\mathrm{FM}}$ holds. As U increases toward the upper limit shown, the Drude weights in both directions are reduced due to increasing insulating tendencies, as discussed before. Reproduced from Ref. [113], Copyright © 2011 American Physical Society.

10   Summary

In this publication, the results gathered by our group in the area of theoretical studies of Hubbard models for the Fe-based superconductors have been reviewed. Results by several other groups were mentioned and cited, but the focus was on our publications that rely on mean-field approximations and computational techniques such as the Lanczos method, and a comparison of our results against a variety of experiments. It has been shown that the Hubbard model presents a region of parameter space

where the ground state properties are in agreement with neutron scattering, photoemission, and transport measurements. In addition, a variety of conceptual issues have been addressed here, and in the cited references, including interorbital pairing tendencies, competition between d and s wave superconductivity, influence of Fe vacancies, possible charge stripe states, nesting effects, and other interesting topics.

The field of Fe-based superconductors is rapidly evolving from the early days where simple weak coupling ideas appeared to work, particularly for 1111 compounds, to the present status where many challenges, such as the presence of superconductors with insulators as parent compound, lead us to revisit notions such as the possible relevance of strong correlations in this type of materials. The study of multiorbital Hamiltonians in this context, such as the Hubbard model, defines a "grand challenge" to theorists since there are few many-body tools available to gather reliable information about these complex models. At present, most of the progress is being made via mean-field approximations, but the next step is to develop more accurate tecniques. The fascinating area of research defined by pnictides and chalcogenides surely will receive the focus of both theorists and experimentalists for a long time, since developing a working theory for high critical temperature superconductors is among the most important conceptual topics of research in condensed matter physics at present.

References and notes

1. Y. Kamihara, T. Watanabe, M. Hirano, and H. Hosono, J. Am. Chem. Soc., 2008, 130(11): 3296

2. G. F. Chen, Z. Li, G. Li, J. Zhou, D. Wu, J. Dong, W. Z. Hu, P. Zheng, Z. J. Chen, H. Q. Yuan, J. Singleton, J. L. Luo, and N. L. Wang, Phys. Rev. Lett., 2008, 101(5): 057007

3. G. F. Chen, Z. Li, D. Wu, G. Li, W. Z. Hu, J. Dong, P. Zheng, J. L. Luo, and N. L. Wang, Phys. Rev. Lett., 2008, 100(24): 247002

4. H. H. Wen, G. Mu, L. Fang, H. Yang, and X. Zhu, Europhys. Lett., 2008, 82(1): 17009

5. X. H. Chen, T. Wu, G. Wu, R. H. Liu, H. Chen, and D. F. Fang, Nature, 2008, 453(7196): 761

6. Z. A. Ren, J. Yang, W. Lu, W. Yi, G. C. Che, X. L. Dong, L. L. Sun, and Z. X. Zhao, Materials Research Innovations, 2008, 12(3): 105

7. Z. A. Ren, W. Lu, J. Yang, W. Yi, X. L. Shen, Z. C. Li, G. C. Che, X. L. Dong, L. L. Sun, F. Zhou, and Z. X. Zhao, Chin. Phys. Lett., 2008, 25(7): 2215

8. Z. A. Ren, G. C. Che, X. L. Dong, J. Yang, W. Lu, W. Yi, X. L. Shen, Z. C. Li, L. L. Sun, F. Zhou, and Z. X. Zhao, Europhys. Lett., 2008, 83(1): 17002

9. E. Dagotto, Rev. Mod. Phys., 1994, 66(3): 763

10. L. Boeri, O. V. Dolgov, and A. A. Golubov, Phys. Rev. Lett., 2008, 101(2): 026403

11. S. Higashitaniguchi, M. Seto, S. Kitao, Y. Kobayashi, M. Saito, R. Masuda, T. Mitsui, Y. Yoda, Y. Kamihara, M. Hirano, and H. Hosono, Phys. Rev. B, 2008, 78(17): 174507

12. A. D. Christianson, M. D. Lumsden, O. Delaire, M. B. Stone, D. L. Abernathy, M. A. McGuire, A. S. Sefat, R. Jin, B. C. Sales, D. Mandrus, E. D. Mun, P. C. Canfield, J. Y. Y. Lin, M. Lucas, M. Kresch, J. B. Keith, B. Fultz, E. A. Goremychkin, and R. J. McQueeney, Phys. Rev. Lett., 2008, 101(15): 157004

13. A. S. Sefat, M. A. McGuire, B. C. Sales, R. Jin, J. Y. Howe, and D. Mandrus, Phys. Rev. B, 2008, 77(17): 174503

14. R. H. Liu, G. Wu, T. Wu, D. F. Fang, H. Chen, S. Y. Li, K. Liu, Y. L. Xie, X. F. Wang, R. L. Yang, L. Ding, C. He, D. L. Feng, and X. H. Chen, Phys. Rev. Lett., 2008, 101(8): 087001

15. K. Haule, J. H. Shim, and G. Kotliar, Phys. Rev. Lett., 2008, 100(22): 226402

16. K. Haule and G. Kotliar, New J. Phys., 2009, 11(2): 025021

17. A. Dubroka, K. W. Kim, M. Rössle, V. K. Malik, A. J. Drew, R. H. Liu, G. Wu, X. H. Chen, and C. Bernhard, Phys. Rev. Lett., 2008, 101(9): 097011

18. A. V. Boris, N. N. Kovaleva, S. S. A. Seo, J. S. Kim, P. Popovich, Y. Matiks, R. K. Kremer, and B. Keimer, Phys. Rev. Lett., 2008, 102(2): 027001

19. C. Liu, T. Kondo, M. E. Tillman, R. Gordon, G. D. Samolyuk, Y. Lee, C. Martin, J. L. McChesney, S. Bud'ko, M. A. Tanatar, E. Rotenberg, P. C. Canfield, R. Prozorov, B. N. Harmon, and A. Kaminski, arXiv:0806.2147, 2008

20. J. Zhao, Q. Huang, C. de la Cruz, S. Li, J. W. Lynn, Y. Chen, M. A. Green, G. F. Chen, G. Li, Z. Li, J. L. Luo, N. L. Wang, and P. Dai, Nat. Mater., 2008, 7(12): 953

21. Y. Kohama, Y. Kamihara, H. Kawaji, T. Atake, M. Hirano, and H. Hosono, J. Phys. Soc. Jpn., 2008, 77(9): 094715

22. K. Nakamura, R. Arita, and M. Imada, J. Phys. Soc. Jpn., 2008, 77(9): 093711

23. H. Liu, W. Zhang, L. Zhao, X. Jia, J. Meng, G. Liu, X. Dong, G. F. Chen, J. L. Luo, N. L. Wang, W. Lu, G. Wang, Y. Zhou, Y. Zhu, X. Wang, Z. Zhao, Z. Xu, C. Chen, and X. J. Zho, Phys. Rev. B, 2008, 78(18): 184514

24. H. J. Grafe, D. Paar, G. Lang, N. J. Curro, G. Behr, J. Werner, J. Hamann-Borrero, C. Hess, N. Leps, R. Klingeler, and B. Büchner, Phys. Rev. Lett., 2008, 101(4): 047003

25. K. Matano, Z. A. Ren, X. L. Dong, L. L. Sun, Z. X. Zhao, and G. Q. Zheng, Europhys. Lett., 2008, 83(5): 57001

26. A. Kawabata, S. C. Lee, T. Moyoshi, Y. Kobayashi, and M. Sato, J. Phys. Soc. Jpn., 2008, 77(10): 103704

27. Y. Ishida, T. Shimojima, K. Ishizaka, T. Kiss, M. Okawa, T. Togashi, S. Watanabe, X. Y. Wang, C. T. Chen, Y. Kamihara, M. Hirano, H. Hosono, and S. Shin, Phys. Rev. B, 2009, 79(6): 060503

28. T. Sato, S. Souma, K. Nakayama, K. Terashima, K. Sugawara, T. Takahashi, Y. Kamihara, M. Hirano, and H. Hosono, J. Phys. Soc. Jpn., 2008, 77(6): 063708

29. H. Y. Liu, X. W. Jia, W. T. Zhang, L. Zhao, J. Q. Meng, G. D. Liu, X. L. Dong, G. Wu, R. H. Liu, X. H. Chen, Z. A. Ren, Y. Wei, G. C. Che, G. F. Chen, N. L. Wang, G. L. Wang, Y. Zhou, Y. Zhu, X. Y. Wang, Z. X. Zhao, Z. Y. Xu, C. T. Chen, and X. J. Zhou, Chin. Phys. Lett., 2008, 25: 3761

30. L. Zhao, H. Liu, W. Zhang, J. Meng, X. Jia, G. Liu, X. Dong, G. F. Chen, J. L. Luo, N. L. Wang, G. Wang, Y. Zhou, Y. Zhu, X. Wang, Z. Zhao, Z. Xu, C. Chen, and X. J. Zhou, Chin. Phys. Lett., 2008, 25: 4402

31. L. Shan, Y. Wang, X. Zhu, G. Mu, L. Fang, and H. H. Wen, Europhys. Lett., 2008, 83(5): 57004

32. G. Mu, X. Zhu, L. Fang, L. Shan, C. Ren, and H. H. Wen, Chin. Phys. Lett., 2008, 25(11): 2221

33. C. Ren, Z. S. Wang, H. Yang, X. Zhu, L. Fang, G. Mu, L. Shan, and H. H. Wen, arXiv:0804.1726, 2008

34. K. Ahilan, F. L. Ning, T. Imai, A. S. Sefat, R. Jin, M. A. McGuire, B. C. Sales, and D. Mandrus, Phys. Rev. B, 2008, 78(10): 100501(R)

35. Y. Nakai, K. Ishida, Y. Kamihara, M. Hirano, and H. Hosono, J. Phys. Soc. Jpn., 2008, 77(7): 073701

36. Y. Wang, L. Shan, L. Fang, P. Cheng, C. Ren, and H. H. Wen, Supercond. Sci. Technol., 2009, 22(1): 015018

37. H. Mukuda, N. Terasaki, H. Kinouchi, M. Yashima, Y. Kitaoka, S. Suzuki, S. Miyasaka, S. Tajima, K. Miyazawa, P. M. Shirage, H. Kito, H. Eisaki, and A. Iyo, J. Phys. Soc. Jpn., 2008, 77(9): 093704

38. O. Millo, I. Asulin, O. Yuli, I. Felner, Z. A. Ren, X. L. Shen, G. C. Che, and Z. X. Zhao, Phys. Rev. B, 2008, 78(9): 092505

39. X. L. Wang, S. X. Dou, Z. A. Ren, W. Yi, Z. C. Li, Z. X. Zhao, and S. I. K. Lee, J. Phys.: Condens. Matter, 2009, 21(20): 205701

40. K. Hashimoto, T. Shibauchi, T. Kato, K. Ikada, R. Okazaki, H. Shishido, M. Ishikado, H. Kito, A. Iyo, H. Eisaki, S. Shamoto, and Y. Matsuda, Phys. Rev. Lett., 2009, 102(1): 017002

41. T. Kondo, A. F. Santander-Syro, O. Copie, Chang Liu, M. E. Tillman, E. D. Mun, J. Schmalian, S. L. Bud'ko, M. A. Tanatar, P. C. Canfield, and A. Kaminski, Phys. Rev. Lett., 2008, 101(14): 147003

42. H. Ding, P. Richard, K. Nakayama, T. Sugawara, T. Arakane, Y. Sekiba, A. Takayama, S. Souma, T. Sato, T. Takahashi, Z. Wang, X. Dai, Z. Fang, G. F. Chen, J. L. Luo, and N. L. Wang, Europhys. Lett., 2008, 83(4): 47001

43. T. Y. Chen, Z. Tesanovic, R. H. Liu, X. H. Chen, and C. L. Chien, Nature, 2008, 453(7199): 1224

44. D. Parker, O. V. Dolgov, M. M. Korshunov, A. A. Golubov, and I. I. Mazin, Phys. Rev. B, 2008, 78(13): 134524

45. K. Kuroki, S. Onari, R. Arita, H. Usui, Y. Tanaka, H. Kontani, and H. Aoki, Phys. Rev. Lett., 2008, 101(8): 087004

46. I. I. Mazin, D. J. Singh, M. D. Johannes, and M. H. Du, Phys. Rev. Lett., 2008, 101(5): 057003

47. X. Dai, Z. Fang, Y. Zhou, and F. C. Zhang, Phys. Rev. Lett., 2008, 101(5): 057008

48. Q. Han, Y. Chen, and Z. D. Wang, Europhys. Lett., 2008, 82(3): 37007

49. B. Liu and I. Eremin, Phys. Rev. B, 2008, 78(1): 014518

50. P. Lee and X. G. Wen, Phys. Rev. B, 2008, 78(14): 144517

51. T. Yildirim, Phys. Rev. Lett., 2008, 101(5): 057010

52. Q. Si and E. Abraham, Phys. Rev. Lett., 2008, 101: 076401

53. Z. J. Yao, J. X. Li, and Z. D. Wang, New J. Phys., 2009, 11(2): 025009

54. C. Xu, M. Mueller, and S. Sachdev, Phys. Rev. B, 2008, 78(2): 020501 (R)

55. E. Manousakis, J. Ren, S. Meng, and E. Kaxiras, Phys. Rev. B, 2008, 78(20): 205112

56. S. Raghu, X. L. Qi, C. X. Liu, D. J. Scalapino, and S. C. Zhang, Phys. Rev. B, 2008, 77(22): 220503

57. T. Li, J. Phys.: Condens. Matter, 2008, 20(42): 425203

58. K. Seo, B. A. Bernevig, and J. Hu, Phys. Rev. Lett., 2008, 101(20): 206404

59. Y. Ran, F. Wang, H. Zhai, A. Vishwanath, and D. H. Lee, Phys. Rev. B, 2008, 79(1): 014505

60. Y. Zhou, W. Q. Chen, and F. C. Zhang, Phys. Rev. B, 2008, 78(6): 064514

61. J. Lorenzana, G. Seibold, C. Ortix, and M. Grilli, Phys. Rev. Lett., 2008, 101(18): 186402

62. R. Sknepnek and G. Samolyuk, Phys. Rev. B, 2009, 79: 054511

63. M. M. Parish, J. Hu, and B. A. Bernevig, Phys. Rev. B, 2008, 78(14): 144514

64. H. Y. Choi and Y. Bang, arXiv:0807.4604, 2008

65. S. Yang, W. L. You, S. J. Gu, and H. Q. Lin, Chin. Phys. B, 2009, 18(06): 2545

66. M. J. Calderon, B. Valenzuela, and E. Bascones, New J. Phys., 2009, 11(1): 013051

67. M. Daghofer, A. Moreo, J. A. Riera, E. Arrigoni, D. J. Scalapino, and E. Dagotto, Phys. Rev. Lett., 2008, 101(23): 237004

68. Z. H. Wang, H. Tang, Z. Fang, and X. Dai, arXiv:0805.0736, 2008

69. W. L. You, S. J. Gu, G. S. Tian, and H. Q. Lin, arXiv:0807.1493, 2008

70. A. Moreo, M. Daghofer, J. A. Riera, and E. Dagotto, Phys. Rev. B, 2009, 79(13): 134502

71. For an early reference on this topic, see: E. Dagotto and A. Moreo, Phys. Rev. Lett., 1989, 63(19): 2148

72. C. de la Cruz, Q. Huang, J. W. Lynn, Jiying Li, W. Ratcliff II, J. L. Zarestky, H. A. Mook, G. F. Chen, J. L. Luo, and P. Dai, Nature (London), 2008, 453(7197): 899

73. R. Yu, K. T. Trinh, A. Moreo, M. Daghofer, J. A. Riera, S. Haas, and E. Dagotto, Phys. Rev. B, 2009, 79(10): 104510

74. M. Daghofer, A. Nicholson, A. Moreo, and E. Dagotto, Phys. Rev. B, 2010, 81(1): 014511

75. S. L. Yu, J. Kang, and J. X. Li, Phys. Rev. B, 2009, 79(6): 064517

76. For a discussion of this relation in the manganite context, see: E. Dagotto, T. Hotta, and A. Moreo, Phys. Rep., 2001, 344(1–3): 1, and references therein

77. E. Bascones, M. J. Calderón, and B. Valenzuela, Phys. Rev. Lett., 2010, 104(22): 227201

78. T. Nomura and K. Yamada, J. Phys. Soc. Jpn., 2000, 69(6): 1856

79. M. Daghofer, Q. L. Luo, R. Yu, D. X. Yao, A. Moreo, and E. Dagotto, Phys. Rev. B, 2010, 81(18): 180514(R)

80. Q. L. Luo, G. B. Martins, D. X. Yao, M. Daghoffer, R. Yu, A. Moreo, and E. Dagotto, Phys. Rev. B, 2010, 82(10): 104508

81. V. J. Emery, S. A. Kivelson, and J. M. Tranquada, Proc. Natl. Acad. Sci. USA, 1999, 96(16): 8814

82. J. Zaanen and O. Gunnarsson, Phys. Rev. B, 1989, 40(10): 7391

83. D. Poilblanc and T. M. Rice, Phys. Rev. B, 1989, 39(13): 9749

84. K. Machida, Physica C, 1989, 158(1–2): 192

85. M. Kato, K. Machida, H. Nakanishi, and M. Fujita, J. Phys. Soc. Jpn., 19980, 59: 1047

86. T. M. Chuang, M. P. Allan, Jinho Lee, Yang Xie, Ni Ni, S. L. Budko, G. S. Boebinger, P. C. Canfield, and J. C. Davis, Science, 2010, 327(5962): 181

87. Arsenic nuclear quadrupole results also indicate the presence of two charge environments in some 1111 pnictides, see: G. Lang, H. J. Grafe, D. Paar, F. Hammerath, K. Manthey, G. Behr, J. Werner, and B. Büchner, Phys. Rev. Lett., 2010, 104(9): 097001

88. Q. L. Luo, D. X. Yao, A. Moreo, and E. Dagotto, Phys. Rev. B, 2011, 83(17): 174513

89. E. Dagotto and T. M. Rice, Science, 1996, 271(5249): 618, and references therein)

90. A. Nicholson, W. Ge, X. Zhang, J. A. Riera, M. Daghofer, A. M. Oleś, G. B. Martins, A. Moreo, and E. Dagotto, Phys. Rev. Lett., 2011, 106(21): 217002

91. A. Moreo, M. Daghofer, A. Nicholson, and E. Dagotto, Phys. Rev. B, 2009, 80(10): 104507

92. H. Gretarsson, A. Lupascu, J. Kim, D. Casa, T. Gog, W. Wu, S. R. Julian, Z. J. Xu, J. S. Wen, G. D. Gu, R. H. Yuan, Z. G. Chen, N. L. Wang, S. Khim, K. H. Kim, M. Ishikado, I. Jarrige, S. Shamoto, J. H. Chu, I. R. Fisher, and Y. J. Kim, arXiv:1107.2211, 2011

93. F. Bondino, E. Magnano, M. Malvestuto, F. Parmigiani, M. A. McGuire, A. S. Sefat, B. C. Sales, R. Jin, D. Mandrus, E. W. Plummer, D. J. Singh, and N. Mannella, Phys. Rev. Lett., 2008, 101(26): 267001

94. A. Nicholson, Q. L. Luo, W. Ge, J. A. Riera, M. Daghofer, G. B. Martins, A. Moreo, and E. Dagotto, Phys. Rev. B, 2011, 84(9): 094519

95. J. Guo, S. Jin, G. Wang, S. Wang, K. Zhu, T. Zhou, M. He, and X. Chen, Phys. Rev. B, 2010, 82(18): 180520(R)

96. M. H. Fang, H. D. Wang, C. H. Dong, Z. J. Li, C. M. Feng, J. Chen, and H. Q. Yuan, Europhys. Lett., 2011, 94(2): 27009

97. W. Bao, Q. Huang, G. F. Chen, M. A. Green, D. M. Wang, J. B. He, X. Q. Wang, and Y. Qui, Chin. Phys. Lett., 2011, 28(8): 086104

98. This magnetic state may coexist with a non-magnetic one in a nanoscale phase separated arrangement, see: A. Ricci, N. Poccia, G. Campi, B. Joseph, G. Arrighetti, L. Barba, M. Reynolds, M. Burghammer, H. Takeya, Y. Mizuguchi, Y. Takano, M. Colapietro, N. L. Saini, and A. Bianconi, Phys. Rev. B, 2011, 84(6): 060511(R)

99. X. P. Wang, T. Qian, P. Richard, P. Zhang, J. Dong, H. D. Wang, C. H. Dong, M. H. Fang, and H. Ding, Europhys. Lett., 2011, 93(5): 57001

100. K. Wang, H. Lei, and C. Petrovic, Phys. Rev. B, 2011, 83(17): 174503, and references therein

101. C. Cao and J. Dai, Phys. Rev. Lett., 2011, 107(5): 056401

102. C. Cao and J. Dai, Phys. Rev. B, 2011, 83(19): 193104

103. R. Yu, P. Goswami, and Q. Si, arXiv:1104.1445, 2011

104. W. G. Yin, C. H. Lin, and W. Ku, arXiv:1106.0881, 2011

105. A related study also using a spin model can be found in: C. Fang, B. Xu, P. Dai, T. Xiang, and J. Hu, arXiv:1103.4599, 2011

106. W. Lv, W. C. Lee, and P. W. Phillips, arXiv:1105.0432, 2011

107. Q. L. Luo, A. Nicholson, J. A. Riera, D. X. Yao, A. Moreo, and E. Dagotto, Phys. Rev. B, 2011, 84(14): 140506(R)

108. J. H. Chu, J. G. Analytis, K. De Greve, P. L. McMahon, Z. Islam, Y. Yamamoto, and I. R. Fisher, Science, 2010, 329(5993): 824

109. E. C. Blomberg, M. A. Tanatar, A. Kreyssig, N. Ni, A. Thaler, Rongwei Hu, S. L. Bud'ko, P. C. Canfield, A. I. Goldman, and R. Prozorov, Phys. Rev. B, 2011, 83: 134505, and references therein

110. A. Dusza, A. Lucarelli, A. Sanna, S. Massidda, J. H. Chu, I. R. Fisher, and L. Degiorgi, arXiv:1107.0670, 2011

111. B. Valenzuela, E. Bascones, and M. J. Calderón, Phys. Rev. Lett., 2010, 105(20): 207202

112. K. Sugimoto, E. Kaneshita, and T. Tohyama, J. Phys. Soc. Jpn., 2011, 80(3): 033706, and references therein

113. X. T. Zhang and E. Dagotto, Phys. Rev. B, 2011, 84(13): 132505, and references therein